EUROPEAN ORGANIZATION FOR PARTICLE PHYSICS

CERN–PPE/93–38
March 3, 1993

A Determination of $\alpha_s(M_{Z^0})$ at LEP using Resummed QCD Calculations

The OPAL Collaboration

Abstract

The strong coupling constant, α_s, has been determined in hadronic decays of the Z^0 resonance, using measurements of seven observables relating to global event shapes, energy correlations and jet rates. The data have been compared with resummed QCD calculations, which are combined with the $\mathcal{O}(\alpha_s^2)$ theory. The seven measurements agree to about 10%, and the final result, based on a weighted average, is:

$$\alpha_s(M_{Z^0}) = 0.120 \pm 0.006 \ ,$$

where the error includes both experimental and theoretical uncertainties. This value corresponds to renormalization scale $\mu = M_{Z^0}$ and the error includes the uncertainty in this choice of scale. The present measurement complements previous determinations using the $\mathcal{O}(\alpha_s^2)$ QCD matrix elements alone, and yields a compatible result, with comparable errors.

To be submitted to Z. Phys. C

The OPAL Collaboration

P.D. Acton[25], G. Alexander[23], J. Allison[16], P.P. Allport[5], K.J. Anderson[9], S. Arcelli[2], A. Astbury[28], D. Axen[29], G. Azuelos[18,a], G.A. Bahan[16], J.T.M. Baines[16], A.H. Ball[17], J. Banks[16], R.J. Barlow[16], S. Barnett[16], J.R. Batley[5], G. Beaudoin[18], A. Beck[23], G.A. Beck[13], J. Becker[10], T. Behnke[27], K.W. Bell[20], G. Bella[23], P. Bentkowski[18], P. Berlich[10], S. Bethke[11], O. Biebel[3], U. Binder[10], I.J. Bloodworth[1], P. Bock[11], B. Boden[3], H.M. Bosch[11], H. Breuker[8], P. Bright-Thomas[25], R.M. Brown[20], A. Buijs[8], H.J. Burckhart[8], C. Burgard[27], P. Capiluppi[2], R.K. Carnegie[6], A.A. Carter[13], J.R. Carter[5], C.Y. Chang[17], D.G. Charlton[8], S.L. Chu[4], P.E.L. Clarke[25], I. Cohen[23], J.C. Clayton[1], W.J. Collins[5], J.E. Conboy[15], M. Cooper[22], M. Coupland[14], M. Cuffiani[2], S. Dado[22], G.M. Dallavalle[2], S. De Jong[13], L.A. del Pozo[5], H. Deng[17], A. Dieckmann[11], M. Dittmar[4], M.S. Dixit[7], E. do Couto e Silva[12], J.E. Duboscq[8], E. Duchovni[26], G. Duckeck[11], I.P. Duerdoth[16], D.J.P. Dumas[6], P.A. Elcombe[5], P.G. Estabrooks[6], E. Etzion[23], H.G. Evans[9], F. Fabbri[2], M. Fierro[2], M. Fincke-Keeler[28], H.M. Fischer[3], D.G. Fong[17], M. Foucher[17], A. Gaidot[21], O. Ganel[26], J.W. Gary[4], J. Gascon[18], R.F. McGowan[16], N.I. Geddes[20], C. Geich-Gimbel[3], S.W. Gensler[9], F.X. Gentit[21], G. Giacomelli[2], R. Giacomelli[2], V. Gibson[5], W.R. Gibson[13], J.D. Gillies[20], J. Goldberg[22], M.J. Goodrick[5], W. Gorn[4], C. Grandi[2], F.C. Grant[5], J. Hagemann[27], G.G. Hanson[12], M. Hansroul[8], C.K. Hargrove[7], P.F. Harrison[13], J. Hart[8], P.M. Hattersley[1], M. Hauschild[8], C.M. Hawkes[8], E. Heflin[4], R.J. Hemingway[6], R.D. Heuer[8], J.C. Hill[5], S.J. Hillier[8], T. Hilse[10], D.A. Hinshaw[18], J.D. Hobbs[8], P.R. Hobson[25], D. Hochman[26], R.J. Homer[1], A.K. Honma[28,a], R.E. Hughes-Jones[16], R. Humbert[10], P. Igo-Kemenes[11], H. Ihssen[11], D.C. Imrie[25], A.C. Janissen[6], A. Jawahery[17], P.W. Jeffreys[20], H. Jeremie[18], M. Jimack[2], M. Jobes[1], R.W.L. Jones[13], P. Jovanovic[1], C. Jui[4], D. Karlen[6], K. Kawagoe[24], T. Kawamoto[24], R.K. Keeler[28], R.G. Kellogg[17], B.W. Kennedy[15], S. Kluth[5], T. Kobayashi[24], D.S. Koetke[8], T.P. Kokott[3], S. Komamiya[24], L. Köpke[8], J.F. Kral[8], R. Kowalewski[6], J. von Krogh[11], J. Kroll[9], M. Kuwano[24], P. Kyberd[13], G.D. Lafferty[16], R. Lahmann[17], F. Lamarche[18], J.G. Layter[4], P. Leblanc[18], A.M. Lee[17], M.H. Lehto[15], D. Lellouch[26], C. Leroy[18], J. Letts[4], S. Levegrün[3], L. Levinson[26], S.L. Lloyd[13], F.K. Loebinger[16], J.M. Lorah[17], B. Lorazo[18], M.J. Losty[7], X.C. Lou[12], J. Ludwig[10], M. Mannelli[8], S. Marcellini[2], G. Maringer[3], C. Markus[3], A.J. Martin[13], J.P. Martin[18], T. Mashimo[24], P. Mättig[3], U. Maur[3], J. McKenna[28], T.J. McMahon[1], J.R. McNutt[25], F. Meijers[8], D. Menszner[11], F.S. Merritt[9], H. Mes[7], A. Michelini[8], R.P. Middleton[20], G. Mikenberg[26], J. Mildenberger[6], D.J. Miller[15], R. Mir[12], W. Mohr[10], C. Moisan[18], A. Montanari[2], T. Mori[24], M. Morii[24], T. Mouthuy[12,b], B. Nellen[3], H.H. Nguyen[9], M. Nozaki[24], S.W. O'Neale[1], F.G. Oakham[7], F. Odorici[2], H.O. Ogren[12], C.J. Oram[28,a], M.J. Oreglia[9], S. Orito[24], J.P. Pansart[21], B. Panzer-Steindel[8], P. Paschievici[26], G.N. Patrick[20], N. Paz-Jaoshvili[23], P. Pfister[10], J.E. Pilcher[9], J. Pinfold[31], D. Pitman[28], D.E. Plane[8], P. Poffenberger[28], B. Poli[2], A. Pouladdej[6], T.W. Pritchard[13], H. Przysiezniak[18], G. Quast[27], M.W. Redmond[9], D.L. Rees[8], G.E. Richards[16], D. Robinson[8], A. Rollnik[3], J.M. Roney[28,c], E. Ros[8], S. Rossberg[10], A.M. Rossi[2], M. Rosvick[28], P. Routenburg[6], K. Runge[10], O. Runolfsson[8], D.R. Rust[12], M. Sasaki[24], C. Sbarra[8], A.D. Schaile[10], O. Schaile[10], W. Schappert[6], P. Scharff-Hansen[8], P. Schenk[4], B. Schmitt[3], H. von der Schmitt[11], S. Schreiber[3], C. Schwick[27], J. Schwiening[3], W.G. Scott[20], M. Settles[12], T.G. Shears[5], B.C. Shen[4], C.H. Shepherd-Themistocleous[7], P. Sherwood[15], R. Shypit[29], A. Simon[3], P. Singh[13], G.P. Siroli[2], A. Skuja[17], A.M. Smith[8], T.J. Smith[28], G.A. Snow[17], R. Sobie[28,c], R.W. Springer[17], M. Sproston[20], K. Stephens[16], J. Steuerer[28], R. Ströhmer[11], D. Strom[30], T. Takeshita[24,d], P. Taras[18], S. Tarem[26], M. Tecchio[9], P. Teixeira-Dias[11], N. Tesch[3], N.J. Thackray[1], M.A. Thomson[15], E. Torrente-Lujan[22], G. Transtromer[25], N.J. Tresilian[16], T. Tsukamoto[24], M.F. Turner[8], G. Tysarczyk-Niemeyer[11], D. Van den plas[18], R. Van Kooten[27], G.J. VanDalen[4], G. Vasseur[21], C.J. Virtue[7], A. Wagner[27], D.L. Wagner[9], C. Wahl[10], J.P. Walker[1], C.P. Ward[5], D.R. Ward[5], P.M. Watkins[1], A.T. Watson[1], N.K. Watson[8], M. Weber[11], P. Weber[6], P.S. Wells[8], N. Wermes[3], M.A. Whalley[1], G.W. Wilson[4], J.A. Wilson[1], V-H. Winterer[10], T. Wlodek[26], S. Wotton[11], T.R. Wyatt[16], R. Yaari[26], A. Yeaman[13], G. Yekutieli[26], M. Yurko[18], W. Zeuner[8], G.T. Zorn[17].

[1]School of Physics and Space Research, University of Birmingham, Birmingham, B15 2TT, UK
[2]Dipartimento di Fisica dell' Università di Bologna and INFN, Bologna, 40126, Italy
[3]Physikalisches Institut, Universität Bonn, D-5300 Bonn 1, FRG
[4]Department of Physics, University of California, Riverside, CA 92521 USA
[5]Cavendish Laboratory, Cambridge, CB3 0HE, UK
[6]Carleton University, Dept of Physics, Colonel By Drive, Ottawa, Ontario K1S 5B6, Canada
[7]Centre for Research in Particle Physics, Carleton University, Ottawa, Ontario K1S 5B6, Canada
[8]CERN, European Organisation for Particle Physics, 1211 Geneva 23, Switzerland
[9]Enrico Fermi Institute and Department of Physics, University of Chicago, Chicago Illinois 60637, USA
[10]Fakultät für Physik, Albert Ludwigs Universität, D-7800 Freiburg, FRG
[11]Physikalisches Institut, Universität Heidelberg, Heidelberg, FRG
[12]Indiana University, Dept of Physics, Swain Hall West 117, Bloomington, Indiana 47405, USA
[13]Queen Mary and Westfield College, University of London, London, E1 4NS, UK
[14]Birkbeck College, London, WC1E 7HV, UK
[15]University College London, London, WC1E 6BT, UK
[16]Department of Physics, Schuster Laboratory, The University, Manchester, M13 9PL, UK
[17]Department of Physics, University of Maryland, College Park, Maryland 20742, USA
[18]Laboratoire de Physique Nucléaire, Université de Montréal, Montréal, Quebec, H3C 3J7, Canada
[20]Rutherford Appleton Laboratory, Chilton, Didcot, Oxfordshire, OX11 0QX, UK
[21]DAPNIA/SPP, Saclay, F-91191 Gif-sur-Yvette, France
[22]Department of Physics, Technion-Israel Institute of Technology, Haifa 32000, Israel
[23]Department of Physics and Astronomy, Tel Aviv University, Tel Aviv 69978, Israel
[24]International Centre for Elementary Particle Physics and Dept of Physics, University of Tokyo, Tokyo 113, and Kobe University, Kobe 657, Japan
[25]Brunel University, Uxbridge, Middlesex, UB8 3PH UK
[26]Nuclear Physics Department, Weizmann Institute of Science, Rehovot, 76100, Israel
[27]Universität Hamburg/DESY, II Inst für Experimental Physik, 2000 Hamburg 52, Germany
[28]University of Victoria, Dept of Physics, P O Box 3055, Victoria BC V8W 3P6, Canada
[29]University of British Columbia, Dept of Physics, 6224 Agriculture Road, Vancouver BC V6T 1Z1, Canada
[30]University of Oregon, Dept of Physics, Eugene, Oregon 97403, USA
[31]University of Alberta, Dept of Physics, Edmonton AB T6G 2J1, Canada

[a]Also at TRIUMF, Vancouver, Canada V6T 2A3
[b]Now at Centre de Physique des Particules de Marseille, Faculté des Sciences de Luminy, Marseille
[c]And IPP, University of Victoria, Dept of Physics, P O Box 3055, Victoria BC V8W 3P6, Canada
[d]Also at Shinshu University, Matsumoto 390, Japan

1 Introduction

The measurement of the strong coupling constant, α_s, is a basic test of the strong interaction sector of the Standard Model, Quantum ChromoDynamics (QCD) [1]. The predictions of QCD are governed by just one fundamental coupling strength. It is therefore important to measure α_s in as many different ways as possible, since consistency between the measurements would serve as a test of the theory. Knowledge of the value of α_s and an understanding of QCD are also important ingredients of many electroweak tests at LEP. Furthermore, an accurate determination of α_s is an important constraint in speculations about unification of the electroweak and strong interactions at very high energies (see e.g. Ref. [2]).

The conventional method by which α_s has been determined involves comparing experimental data with QCD calculations based on an order-by-order expansion in powers of α_s. In the case of the process $e^+e^- \longrightarrow$ hadrons the QCD matrix elements are fully known to $\mathcal{O}(\alpha_s^2)$ [3], corresponding to final states containing no more than four partons. Predictions for the distributions of many observables to $\mathcal{O}(\alpha_s^2)$ based on these matrix elements have been given in Ref. [4]. In a recent publication [5] the OPAL collaboration determined $\alpha_s(M_{Z^0})$ from 13 different observables in $\mathcal{O}(\alpha_s^2)$, and after making reasonable estimates of experimental and theoretical uncertainties found that the values were compatible. The final uncertainty on the value of $\alpha_s(M_{Z^0})$ was about 5%, the accuracy being mainly limited by theoretical uncertainties, particularly relating to higher order effects and hadronization. Other measurements of α_s at LEP to $\mathcal{O}(\alpha_s^2)$ have been presented in Refs. [6]–[17]. Measurements of α_s at LEP to $\mathcal{O}(\alpha_s^3)$ using the total hadronic cross-section and the hadronic decays of the τ-lepton are summarised in Refs. [18, 19].

This standard procedure, based on the $\mathcal{O}(\alpha_s^2)$ matrix elements, is unsuccessful in describing the back-to-back two-jet region of phase space. In this region multiple emissions of soft gluons may be expected to be important. An alternative approach may be taken to the QCD calculations of hadronic final states in e^+e^- annihilations, based on the resummation of leading logarithms which arise from soft and collinear singularities in gluon emission. The consequence is that the effective expansion parameter is not simply α_s, but $\alpha_s L^2$ (to leading order in L), where $L = \ln(1/y)$ and y is some generic observable which tends to zero in the two-jet region. At small y the value of $\alpha_s L^2$ is not small, and therefore these terms must be summed to all orders in α_s in order to provide a satisfactory calculation. For certain observables it has proved possible to sum both the leading and next-to-leading logarithms, which we refer to as the "Next-to-Leading Log Approximation" or NLLA. In the present paper we consider seven observables describing the final state in $e^+e^- \longrightarrow$ hadrons for which NLLA calculations are available: thrust [20, 21], heavy jet mass [22, 21], two measures of jet broadening [23], energy-energy correlations [24, 25], two-jet rates [26] and average jet multiplicities [27] (though in the latter two cases the next-to-leading terms have been only partially resummed). First results using the thrust and heavy jet mass observables were given in a previous OPAL paper [5], and other analyses of LEP data in the NLLA framework have been presented in Refs. [28, 29, 30]. A recent compilation of measurements of α_s based on both the $\mathcal{O}(\alpha_s^2)$ and the NLLA approaches is given in Ref. [18].

The NLLA calculations are expected to be most reliable in predicting the parton distributions in the two-jet region. Unfortunately this region is subject to particularly large hadronization effects, which introduce significant uncertainties when confronting the theory with data. We therefore do not determine α_s simply from the NLLA calculations. Instead the NLLA calculation is combined with the $\mathcal{O}(\alpha_s^2)$ matrix element approach to provide a calculation which includes the full knowledge of the $\mathcal{O}(\alpha_s^2)$ terms, together with the leading and next-to-leading logarithmic parts of the higher order terms in α_s. One expects that this will provide a more complete calculation than either the $\mathcal{O}(\alpha_s^2)$ or the NLLA approach separately, and might therefore allow a reduction in the systematic error in

α_s. We explore this possibility in the present paper. By applying the method to a wider range of observables than has hitherto been possible we can look for consistency between the different values of α_s obtained, which will give an indication of the reliability of this approach to the QCD calculations. By comparing the results with those from the conventional $\mathcal{O}(\alpha_s^2)$ technique we hope to gain further insight into higher order effects.

The present paper is organized as follows: a brief account of the OPAL detector and the data selection procedures is given in Sect. 2, and the observables used and the methods adopted for correcting the data are described in Sect. 3. The application of the NLLA and $\mathcal{O}(\alpha_s^2)$ QCD calculations to the determination of α_s is presented in Sect. 4. Finally Sect. 5 contains a summary and some discussion of the results.

2 The OPAL Detector and Data Selection

A detailed description of the OPAL detector has been presented in Ref. [31], and therefore only a short account of some of its features relevant to the present analysis will be given here.

The momenta of charged particles are measured in the central tracking detectors. For this analysis we use three drift chamber systems. A precision vertex chamber, of radius 24 cm and length 100 cm provides space points with resolution about 50 μm in the $r-\phi$ plane*. This is surrounded by a large jet chamber, of radius 185 cm and length about 400 cm, which provides up to 159 digitizations with an $r-\phi$ resolution of around 130 μm. Outside this lies a system of z-chambers, to improve the resolution in θ. The central detector lies within an axial magnetic field of 0.435 T.

The electromagnetic calorimeter consists of a barrel of 9440 lead glass blocks oriented so that they nearly point to the interaction region, and two endcaps of 1132 lead glass blocks each, aligned along the z-axis. Each block subtends approximately 40×40 mrad^2 at the origin, and the overall coverage is about 98% of 4π. In addition to measuring the energies of electrons and photons, the electromagnetic calorimeter records a significant fraction of the energy of charged and neutral hadrons.

The OPAL trigger [32] has a high degree of redundancy, so that the efficiency for accepting multihadronic events is extremely high, greater than 99.9%. The online filter and offline selection procedures are described in Refs. [33, 34], and are again highly efficient. For the present analysis further cuts were applied to remove residual background and provide a sample of well contained events. The collision energy was required to lie within 0.5 GeV of the Z^0 mass, and those parts of the detector essential for the present analysis (central detector and electromagnetic calorimeter) were required to be fully operational. Charged tracks accepted for this analysis were required to satisfy the following criteria: transverse momentum with respect to the collision axis greater than 0.15 GeV/c, at least 40 reconstructed points in the jet chamber, extrapolation to the collision point within 2 cm in $r-\phi$ and 25 cm in z and measured momentum less than 60 GeV/c. The number of such tracks was required to be at least five to reduce $\tau^+\tau^-$ background. Clusters of electromagnetic energy were used if their observed energy was greater than 0.25 GeV, and known noisy channels in the detector were removed. The thrust axis (Sect. 3.1) was determined using all tracks and clusters satisfying these criteria, and required to fulfil the condition $|\cos\theta| < 0.9$ in order that the event be well contained. Using these selection criteria, Monte Carlo studies indicate that, within the chosen range of $\cos\theta$, 99.86$\pm$0.07% of hadronic Z^0 decays are accepted, with a contamination of about 0.14% from $\tau^+\tau^-$ events, and around

*The OPAL coordinate system is defined so that z is the coordinate parallel to the e^- beam, r is the coordinate normal to this axis, θ is the polar angle with respect to z and ϕ is the azimuthal angle about the z-axis.

0.07% from two-photon interactions. Using the OPAL data collected in 1990 and 1991 a data sample of 336 247 events remained for analysis after these cuts.

3 Experimental Procedure

3.1 The Observables used for Analysis

Our determination of α_s is based on measurements of the following variables, for all of which resummed QCD calculations are available:

Thrust: The thrust T is defined [35] by

$$T = \max_{\hat{\boldsymbol{n}}} \left(\frac{\sum_i |\boldsymbol{p}_i \cdot \hat{\boldsymbol{n}}|}{\sum_i |\boldsymbol{p}_i|} \right); \tag{1}$$

where i runs over all the final state particles, and the axis $\hat{\boldsymbol{n}}$ is chosen to maximize the value of the expression in parentheses; this axis $\hat{\boldsymbol{n}}_T$ is referred to as the thrust axis. In the present analysis we use the observable $(1-T)$, which tends to zero in the two-jet region.

Heavy Jet Mass: This variable has been proposed in Ref. [36]. We divide the particles in an event into two groups by the plane orthogonal to the thrust axis, $\hat{\boldsymbol{n}}_T$, and compute the invariant mass of each group. We define the heavier mass to be M_H. For the determination of α_s we use the scaled variable $M_H/\sqrt{s}$, where s is the square of the centre-of-mass energy. In our previous publication [5] we also considered an alternative way of separating the particles into two groups. It transpired that the results from the two approaches, including all their systematic errors, were virtually identical, so in the current study we use only the simpler method based on the thrust axis. To first order in α_s the heavy jet mass and thrust are related by $(1-T) = M_H^2/s$.

Jet Broadening measures: These observables have been suggested in Ref. [23]. Again the event is divided into two hemispheres, $S_\pm$, by the plane orthogonal to the thrust axis, $\hat{\boldsymbol{n}}_T$. In each hemisphere, the quantity:

$$B_\pm = \frac{\sum\limits_{i \in S_\pm} |\boldsymbol{p}_i \times \hat{\boldsymbol{n}}_T|}{2 \sum\limits_i |\boldsymbol{p}_i|} \tag{2}$$

is computed, where the sum in the denominator runs over all particles, whilst that in the numerator runs over one hemisphere. The observables used for the study of α_s are

$$B_T = B_+ + B_- \qquad \text{and} \qquad B_W = \max(B_+, B_-) \quad , \tag{3}$$

referred to as the "total jet broadening" and "wide jet broadening" respectively. To leading order in α_s, $B_T = B_W = \frac{1}{2}O$ (where O is the oblateness [37]). Both B_T and B_W tend to zero in the two-jet region. These variables are sensitive to the transverse structure of jets, and may therefore be complementary to $(1-T)$ and $M_H/\sqrt{s}$, which are more dependent on the longitudinal momenta.

Energy-Energy Correlation: The energy-energy correlation function Σ_{EEC} [38] is defined in terms of the angle χ_{ij} between two particles i and j in a multihadronic event:

$$\Sigma_{EEC}(\chi) = \frac{1}{\Delta\chi \cdot N} \sum_N \int_{\chi - \frac{1}{2}\Delta\chi}^{\chi + \frac{1}{2}\Delta\chi} \sum_{i,j} \frac{E_i E_j}{E_{vis}^2} \cdot \delta(\chi' - \chi_{ij})\, d\chi' \,, \tag{4}$$

where E_i and E_j are the energies of particles i and j, E_{vis} is the sum over the energies of all particles in the event, $\Delta\chi$ is the angular bin width and N is the total number of events. The normalization ensures that the integral of $\Sigma_{EEC}(\chi)$ from $\chi = 0°$ to $180°$ is unity.

Jet Rates: For the present analysis we define jets through the "Durham" scheme [26, 39, 40]. A jet resolution variable y_{ij} is defined for each pair of particles i and j by:

$$y_{ij} = \frac{2\min(E_i^2, E_j^2)(1-\cos\theta_{ij})}{E_{vis}^2} \quad , \tag{5}$$

where E_i and E_j are the energies of the two particles or jets i and j, θ_{ij} is the angle between them and E_{vis} is again the sum over the energies of all particles in the event. If the smallest value of y_{ij} is smaller than some cutoff y_{cut} then particles i and j are replaced by the sum of their four-momenta. The process is repeated until all remaining pairs satisfy $y_{ij} > y_{cut}$, and the groups of particles at this stage are called "jets". Resummed QCD calculations are available for two observables related to these jet rates; the two-jet rate:

$$R_2 = \frac{\sigma_{2-jet}}{\sigma_{tot}}$$

and the average number of jets:

$$\mathcal{N} = \frac{1}{\sigma_{tot}}\sum_{n=2}^{\infty} n\sigma_{n-jet}$$

as a function of y_{cut} in both cases. When performing fits to the data we have used the differential jet rate $D_2(y_{cut}) \equiv dR_2(y_{cut})/dy_{cut}$ instead of R_2.

3.2 Correction of Data

The observables described above were calculated from the data using both charged tracks and clusters of electromagnetic energy. A Monte Carlo simulation of the OPAL detector [41] was then used in order to correct for experimental resolution and acceptance. In this correction the effects of initial state photon radiation were also removed, although these effects are small since only data at the Z^0 peak energy were used. The data were further corrected for the effects of hadronization using QCD parton shower Monte Carlo models. The procedure closely followed Ref. [42]. The simplest technique employed bin-by-bin correction factors. Two Monte Carlo samples were used: a sample (I) with no initial state photon radiation and no detector simulation, and a sample (II) using the same Monte Carlo but including detector simulation and initial-state radiation. The QCD parton shower model JETSET [43], version 7.3, with parameters tuned to OPAL data on global event shapes [42], was used to derive the default correction factors. The events of sample (II) were processed by the same reconstruction programs and subjected to the same event selection cuts as the real data. Defining $\mathcal{T}_i$ to be the value of the quantity which is being investigated (e.g. the normalized differential cross-section) in bin i of a distribution for sample (I), and $\mathcal{D}_i$ to be the corresponding quantity for the events which survive after event reconstruction and selection, in sample (II), the correction factor $\mathcal{K}_i$ for bin i is then given by $\mathcal{K}_i = \mathcal{T}_i/\mathcal{D}_i$. The experimental measurement, for bin i of the distribution, is corrected by multiplying it by the factor $\mathcal{K}_i$. The distribution for the Monte Carlo sample (I) may be computed using the stable particles (those with lifetimes greater than $3 \cdot 10^{-10}$ s), in which case the procedure corrects only for detector effects, and we refer to these as data corrected to the *hadron level*. Alternatively, if the partons in sample (I) are used instead then the correction procedure accounts for both detector effects and hadronization, and we refer to these as data corrected to the *parton level*. We use the expression *detector level* to refer to the uncorrected data.

As discussed in Ref. [42], this simple bin-by-bin correction procedure is reliable only if the bin width selected for the data is greater than or comparable with the experimental resolution, so that migration between bins is small. In the case of the event shape variables $(1-T)$, M_H, B_T and B_W the effective resolution resulting from hadronization and detector effects is quite large, which requires that a large bin width be employed in the bin-by-bin procedure. Therefore an alternative approach was adopted for these observables in order to be able to use a somewhat finer binning. Using the events in sample (II) which pass the selection criteria at the detector level, one can compute the matrix P, in which the element P_{ji} gives the probability that an event in bin i at the hadron (or parton) level is found to lie in bin j when the detected tracks and clusters are used. Then, if C_i is the number of events in bin i at the hadron (or parton) level, we may infer the probability Q_{ij} that an event found in bin j at the detector level originated from bin i at the hadron (or parton) level:

$$Q_{ij} = \frac{P_{ji}C_i}{\sum_k P_{jk}C_k} \quad . \tag{6}$$

The data may then be corrected to the hadron (or parton) level by:

$$C_i' = \sum_j Q_{ij} D_j \quad , \tag{7}$$

where D_j is the number of observed events in bin j in the data. It is clear from eqn.(6) that the matrix Q depends on the true distribution C, initially taken from the Monte Carlo. If the corrected data C_i' differ significantly from the assumed distribution C_i, then C_i' may be substituted for C_i in eqn.(6) and the correction procedure iterated. It was found that the value of α_s was extremely stable under such an iterative procedure, as expected since the Monte Carlo was already tuned to fit the data well. Finally a bin-by-bin correction was applied to account for the effects of initial state radiation and losses of events in the selection procedure – this correction turned out to be very small. We found that the data corrected using this matrix method yielded values of α_s which were entirely compatible with those from the bin-by-bin method. Therefore we show the matrix corrected results for $(1-T)$, M_H, B_T and B_W in this paper.

In Table 1 we present data for the observables used in the present analyses, corrected for detector effects (i.e. at the hadron level). The errors include a statistical part, arising from finite statistics in both data and Monte Carlo, and a (dominant) contribution from experimental systematic effects, estimated as described in Sect. 4.3. The errors are in general correlated between bins; these effects were estimated by dividing the data and Monte Carlo samples into a number of independent subsets and computing the covariance matrix. The errors quoted in Table 1 are based on the diagonal terms of the covariance matrix, but the full matrix was available when fitting the data. In Fig. 1 we show the hadron level data for the observables which we have not presented in previous publications [5, 8], namely B_T, B_W and $\mathcal{N}$, compared with the predictions of the parton shower models JETSET version 7.3 [43] and HERWIG version 5.5 [44], with parameters tuned to OPAL data as described in Ref. [42, 45].

4 Determination of α_s

4.1 Combination of Resummed and Fixed Order QCD Calculations

For the present analysis, the NLLA and $\mathcal{O}(\alpha_s^2)$ calculations have to be combined before they are fitted to data. There are a number of different schemes by which this may be done, which we describe here, following the discussion in Refs.[28, 46, 21]. We consider four schemes, which we refer to as '$\ln(R)$-matching', 'R-matching', 'modified R-matching' and 'modified $\ln(R)$-matching', though not all

schemes are applicable to all seven observables. The various matching schemes all embody the full $\mathcal{O}(\alpha_s^2)$ result, together with the resummation of leading and next-to-leading logarithms, but they differ in higher orders. The technical details of these schemes are given in the remainder of this section.

For all the variables we are considering for which resummation is possible, with the exception of the average jet multiplicity $\mathcal{N}$, the cumulative cross-section may be written in the general form:

$$R(y) \equiv \int_0^y \frac{1}{\sigma}\frac{d\sigma}{dy}dy = C(\alpha_s)\exp G(\alpha_s, L) + D(\alpha_s, y) \quad , \tag{8}$$

where y is $(1-T)$, M_H^2/s, B_T or B_W in the case of the event shapes, $\cos^2(\frac{\chi}{2})$ in the case of Σ_{EEC}[†], and y_{cut} for the jet rates, and $L = \ln(1/y)$. $D(\alpha_s, y)$ is a remainder function which should vanish as $y \to 0$. The general structure of the cross-section in powers of α_s and of large logarithms is indicated in Table 2. The functions C and G may be written:

$$C(\alpha_s) = 1 + \sum_{n=1}^{\infty} C_n {\overline{\alpha}_s}^n \tag{9}$$

and

$$G(\alpha_s, L) = \sum_{n=1}^{\infty}\sum_{m=1}^{n+1} G_{nm}{\overline{\alpha}_s}^n L^m \equiv Lg_1(\alpha_s L) + g_2(\alpha_s L) + \alpha_s g_3(\alpha_s L) + \alpha_s^2 g_4(\alpha_s L)\cdots \quad , \tag{10}$$

where for brevity we write $\overline{\alpha}_s$ for $(\alpha_s/2\pi)$. The functions $Lg_1(\alpha_s L)$ and $g_2(\alpha_s L)$ represent the sums of the leading and next-to-leading logarithms respectively, to all orders in α_s (see Table 2). The NLLA calculations give an approximate expression for $R(y)$ in the form:

$$R_{NLLA}(y) = (1 + C_1\overline{\alpha}_s + C_2\overline{\alpha}_s^2)\exp[Lg_1(\alpha_s L) + g_2(\alpha_s L)] \quad . \tag{11}$$

The functions g_1 and g_2 are given by the NLLA calculations; the coefficient C_1 is known exactly from the $\mathcal{O}(\alpha_s)$ matrix elements and C_2 is known (in the case of $(1-T)$, M_H, B_T and B_W) from numerical integration of the $\mathcal{O}(\alpha_s^2)$ matrix elements; their values are summarized in Table 3. The full $\mathcal{O}(\alpha_s^2)$ calculation yields an approximate expression for $R(y)$ of the form:

$$R_{\mathcal{O}(\alpha_s^2)}(y) = 1 + \mathcal{A}(y)\overline{\alpha}_s + \mathcal{B}(y)\overline{\alpha}_s^2 \quad , \tag{12}$$

where the coefficients $\mathcal{A}(y)$ and $\mathcal{B}(y)$ are equivalent to the A and B coefficients tabulated in Ref.[4], but integrated to correspond to the cumulative distribution $R(y)$. In the case of Σ_{EEC}, B_T and B_W we have run the program `EVENT`, which was used by the authors of Ref. [4], to derive values of the coefficients.

The simplest matching scheme involves taking the logarithm of eqn.(12) and expanding as a power series, yielding:

$$\ln R_{\mathcal{O}(\alpha_s^2)}(y) = \mathcal{A}(y)\overline{\alpha}_s + [\mathcal{B}(y) - \tfrac{1}{2}\mathcal{A}(y)^2]\overline{\alpha}_s^2 + \mathcal{O}(\alpha_s^3) \quad , \tag{13}$$

and similarly rewriting eqn.(11) as:

$$\ln R_{NLLA}(y) = Lg_1(\alpha_s L) + g_2(\alpha_s L) + C_1\overline{\alpha}_s + [C_2 - \tfrac{1}{2}C_1^2]\overline{\alpha}_s^2 + \mathcal{O}(\alpha_s^3) \quad . \tag{14}$$

Removing the terms to $\mathcal{O}(\alpha_s^2)$ in the NLLA expression eqn.(14), replacing them by the $\mathcal{O}(\alpha_s^2)$ terms from eqn.(13) and neglecting non-logarithmic terms of higher order yields (c.f. Table 2):

$$\begin{aligned} \ln R(y) \;\; = \;\; & Lg_1(\alpha_s L) + g_2(\alpha_s L) - (G_{11}L + G_{12}L^2)\overline{\alpha}_s - (G_{22}L^2 + G_{23}L^3)\overline{\alpha}_s^2 \\ & + \mathcal{A}(y)\overline{\alpha}_s + [\mathcal{B}(y) - \tfrac{1}{2}\mathcal{A}(y)^2]\overline{\alpha}_s^2 \quad . \end{aligned} \tag{15}$$

[†]An additional factor $\frac{1}{2}$ precedes the exponential for Σ_{EEC}, in this and subsequent equations.

This procedure will be referred to as '$\ln(R)$-*matching*'. Alternatively the analogous procedure may be carried out for the functions $R(y)$ instead of $\ln(R(y))$, yielding:

$$\begin{aligned} R(y) &= (1 + C_1\overline{\alpha}_s + C_2\overline{\alpha}_s^2)\exp\{Lg_1(\alpha_s L) + g_2(\alpha_s L)\} - (C_1 + G_{11}L + G_{12}L^2)\overline{\alpha}_s \\ &\quad - [C_2 + G_{22}L^2 + G_{23}L^3 + (G_{11}L + G_{12}L^2)(C_1 + \tfrac{1}{2}(G_{11}L + G_{12}L^2))]\,\overline{\alpha}_s^2 \\ &\quad + \mathcal{A}(y)\overline{\alpha}_s + \mathcal{B}(y)\overline{\alpha}_s^2 \ . \end{aligned} \tag{16}$$

This procedure will be referred to as '*R-matching*'. It would be expected that R-matching would be less reliable than the $\ln(R)$-scheme, because the subleading term $G_{21}\overline{\alpha}_s^2 L$, which does not vanish as $y \to 0$, is not exponentiated in eqn.(16), whereas it is exponentiated in eqn.(15) because it is implicitly included in the $\mathcal{B}(y)$ coefficient. This leads one to consider a modified form of eqn.(16) in which the $G_{21}\overline{\alpha}_s^2 L$ term is included in the argument of the exponential, and subtracted after exponentiation. We refer to this as the '*modified R-matching*' scheme (called 'intermediate' matching in Ref. [28], and R-matching in Ref. [21]). The coefficient G_{21} is not known analytically, but may be inferred approximately from numerical integration of the $\mathcal{O}(\alpha_s^2)$ matrix elements. The relevant G_{nm} coefficients, insofar as they are known, are given in Table 3, based on Ref. [21] for $(1-T)$ and M_H, Ref. [23] for B_T and B_W, Ref. [24] for Σ_{EEC}[‡], and on the expressions in the appendix to Ref. [28] for R_2[§].

A further problem is that the NLLA calculations are not guaranteed to satisfy the necessary constraints, $R(y) \to 1$ and $dR/dy \to 0$, at the kinematic limit, y_{max}, corresponding to the region of hard gluon emission. In consequence the combined NLLA+$\mathcal{O}(\alpha_s^2)$ calculation may fit data less well than the $\mathcal{O}(\alpha_s^2)$ expression in the hard region. It has been proposed [46, 21] that this difficulty could be overcome in the $\ln(R)$-matching scheme by replacing L in the NLLA part of eqn.(15) by $L' = \ln(y^{-1} - y_{max}^{-1} + 1)$. We refer to this possibility as '*modified* $\ln(R)$-*matching*'. [¶]

All four matching schemes described above may be applied to the observables $(1-T)$, M_H, B_T and B_W. The value of G_{21} is not known for R_2, and cannot be estimated until a complete calculation of G_{22} is available, so the modified R-matching scheme is not applicable to R_2. The Σ_{EEC} exhibits a particular problem because the $\mathcal{O}(\alpha_s^2)$ differential distribution diverges at both small and large y, so that the cumulative coefficients $\mathcal{A}$ and $\mathcal{B}$ cannot be reliably determined. This precludes the use of the $\ln(R)$- and modified $\ln(R)$-schemes for Σ_{EEC}. However, the other matching schemes are applicable to the differential Σ_{EEC} distribution because they depend only on differences between values of $\mathcal{A}$ and $\mathcal{B}$ across a bin. It should also be noted that the coefficient C_2 is not known for Σ_{EEC} nor for R_2.

The situation is slightly different in the case of the average jet multiplicity $\mathcal{N}$, since it cannot be written in the exponentiated form of eqn.(8). The calculation to $\mathcal{O}(\alpha_s^2)$ gives a prediction of the form:

$$\mathcal{N}_{\mathcal{O}(\alpha_s^2)} = 2 + A(y)\overline{\alpha}_s + B(y)\overline{\alpha}_s^2 \ , \tag{17}$$

and the NLLA calculation yields:

$$\mathcal{N}_{NLLA} = 2 + \sum_{n=1}^{\infty} \mathcal{H}_n(L)\overline{\alpha}_s{}^n \ ; \ \mathcal{H}_1(L) = H_{12}L^2 + H_{11}L \ ; \ \mathcal{H}_2(L) = H_{24}L^4 + H_{23}L^3 + H_{22}L^2 \ . \tag{18}$$

The equivalent to the R-matching scheme is:

$$\mathcal{N} = \mathcal{N}_{NLLA} - \mathcal{H}_1(L)\overline{\alpha}_s - \mathcal{H}_2(L)\overline{\alpha}_s^2 + A(y)\overline{\alpha}_s + B(y)\overline{\alpha}_s^2 \ , \tag{19}$$

[‡]The calculations of Ref. [24] rather than those of Ref. [25] are used for Σ_{EEC} because the former are in a suitable form for matching to the $\mathcal{O}(\alpha_s^2)$ calculations.

[§]It should be noted that the coefficient G_{22} for the R_2 variable is not expected to be correct, since not all next-to-leading terms have been resummed in this case; the value given in Table 3 is simply the coefficient of $\overline{\alpha}_s^2 L^2$ in the expansion of the expression given in Ref. [28], which should be the correct value to use in the matching procedure.

[¶]The value of y_{max} was taken to be 0.5 for $(1-T)$, 0.42 for $M_H/\sqrt{s}$, 0.41 for B_T, 0.325 for B_W and 0.333 for R_2. The actual kinematic limit depends on the number of partons in the final state, and is not precisely known for some of the variables. However, the fitted values of α_s were found to be insensitive to the precise value chosen for y_{max}.

while a procedure analogous to $\ln(R)$-matching is [47]:

$$\mathcal{N} = \mathcal{N}_{NLLA} \exp\{-\mathcal{H}_1(L)\overline{\alpha}_s - (\mathcal{H}_2(L) - \tfrac{1}{2}\mathcal{H}_1(L)^2)\overline{\alpha}_s^2 + A(y)\overline{\alpha}_s + (B(y) - \tfrac{1}{2}A(y)^2)\overline{\alpha}_s^2\} \quad . \tag{20}$$

The coefficients H_{12}, H_{11}, H_{24} and H_{23} are contained in eqn.(8) of Ref. [27], and by expansion of the NLLA expressions in Ref. [27] one can obtain $H_{22} = \frac{40}{6561} n_f(7n_f - 27)$ [47].

A final consideration is the choice of renormalization scale. To $\mathcal{O}(\alpha_s^2)$ the strong coupling constant may be written (following the convention of Ref. [48]):

$$\alpha_s(\mu) = \frac{1}{\beta_0 \ln(\mu^2/\Lambda^2_{\overline{MS}})}\left[1 - \frac{\beta_1 \ln(\ln(\mu^2/\Lambda^2_{\overline{MS}}))}{\beta_0^2 \ln(\mu^2/\Lambda^2_{\overline{MS}})}\right] \quad , \tag{21}$$

where $\beta_0 = (33-2n_f)/12\pi$, $\beta_1 = (153-19n_f)/24\pi^2$ and n_f is the number of quark flavours, taken to be 5. The QCD scale $\Lambda_{\overline{MS}}$ refers to the $\overline{MS}$ renormalization scheme. One can relate the renormalization scale μ to the e^+e^- centre of mass energy by

$$\mu = x_\mu \cdot E_{cm}, \tag{22}$$

where x_μ is the renormalization scale factor. Naïvely x_μ would be expected to be of order unity. However, using $\mathcal{O}(\alpha_s^2)$ QCD the experimental data for most observables tend to be better fitted with a value $x_\mu \ll 1$ (see e.g. Ref. [5]). This is generally understood to be a consequence of missing higher order terms in the $\mathcal{O}(\alpha_s^2)$ approach, and it is therefore anticipated that the inclusion of higher order terms in the NLLA calculations should reduce the dependence on x_μ. In order to account for the dependence on x_μ, the above formulæ have to be modified by the replacements [4, 21]:

$$\begin{aligned}
\mathcal{B}(y) &\longrightarrow \mathcal{B}(y) + \mathcal{A}(y) 2\pi\beta_0 \ln x_\mu^2 \\
g_2(\alpha_s L) &\longrightarrow g_2(\alpha_s L) + \beta_0 \alpha_s^2 L^2 \frac{dg_1(\alpha_s L)}{d(\alpha_s L)} \ln x_\mu^2 \\
G_{22} &\longrightarrow G_{22} + 2\pi\beta_0 G_{12} \ln x_\mu^2 \quad .
\end{aligned} \tag{23}$$

An equivalent procedure for $\mathcal{N}$ [47] involves substituting throughout:

$$\overline{\alpha}_s \longrightarrow \overline{\alpha}_s + \overline{\alpha}_s^2 2\pi\beta_0 \ln x_\mu^2 \quad . \tag{24}$$

4.2 Measurement of $\alpha_s(M_{Z^0})$

After correcting the data to the parton level as outlined in Sect. 3.2, the NLLA+$\mathcal{O}(\alpha_s^2)$ QCD calculations were fitted to the data using a least χ^2 method. For comparison we also fitted the $\mathcal{O}(\alpha_s^2)$ QCD predictions. A number of considerations were taken into account in determining the range over which the data were to be fitted. We required that the detector and hadronization correction factors should be reasonably uniform across the fit range, and that the hadronization correction should not be strongly model dependent. This generally determined how far into the two-jet region ($y \to 0$) the NLLA fits could reliably be performed, and also set the upper limit on most of the $\mathcal{O}(\alpha_s^2)$ fits. We also required that the value of χ^2 be "reasonable", in the sense that the contributions to χ^2 should be distributed fairly evenly across the fit range, and not dominated by the extreme bins. Generally the lower limit for the $\mathcal{O}(\alpha_s^2)$ fits had to be placed higher (further from the two jet region) than for the NLLA fits, and in some cases the upper limit had to be placed lower for the NLLA fits than for the $\mathcal{O}(\alpha_s^2)$ fits (because the NLLA calculations do not necessarily fall off correctly toward the hard kinematic limit). A further constraint for Σ_{EEC} was the presence of an unphysical pole introduced in the NLLA calculation [24], at around $\chi = 178°$; the chosen fit range was well away from this point.

The fit ranges chosen are given in Table 4. We confirmed that the results for α_s were not significantly altered if the fit range was moved by one or two bins (though in some cases the value of χ^2 was significantly worse), and therefore no additional error was assigned resulting from possible uncertainties in the choice of fit range.

Only statistical errors on the data were included in the calculation of χ^2 (including the effect of limited Monte Carlo statistics). Systematic uncertainties on the data (Sect. 4.3.1) were not taken into account in calculating χ^2 since their definition is essentially arbitrary, and their correlations could not be estimated reliably. Nor were errors on the QCD coefficients taken into account. Fits were performed with the renormalization scale factor x_μ fixed to 1, and also with x_μ treated as an additional free parameter. When using a value $x_\mu \neq 1$ the fitted value of $\Lambda_{\overline{MS}}$ is converted into an equivalent value of α_s at scale M_{Z^0} using eqn.(21); throughout the rest of this paper α_s should be taken to refer to $\alpha_s(M_{\mathrm{Z}^0})$. We used the $\ln(R)$-matching scheme to combine the NLLA and $\mathcal{O}(\alpha_s^2)$ calculations, except for Σ_{EEC} where the modified R-matching scheme was used instead. The use of other matching schemes will be discussed in detail below. The fit results are listed in Table 5. The data corrected to the parton level are shown in Figs. 2 and 3, with the NLLA+$\mathcal{O}(\alpha_s^2)$ fits superimposed. The dependence of α_s and χ^2/d.o.f. on x_μ is shown in Fig. 4. The fits with $x_\mu = 1$ yield acceptable values of χ^2/d.o.f. (less than 10 for all observables except B_W), though they are all greater than unity, as might be expected since the theory is known to lack some higher order terms, and also since experimental systematic errors have not been included at this stage. In the case of M_H, B_W and B_T the theory is seen to diverge from the data at high values; this arises because the NLLA calculations are not constrained to fall to zero at the upper kinematic limit; the introduction of the modified $\ln(R)$-matching scheme substantially reduces this problem. Five of the observables give very similar values of α_s, while B_W gives a rather lower value, and Σ_{EEC} a higher result. In the fits where x_μ is treated as a free parameter, we find that only the jet broadening measures favour values of x_μ much smaller than one, while several observables yield a best fit with $x_\mu > 1$. The dependence of χ^2/d.o.f. on x_μ is particularly weak for $(1-T)$ and R_2, so that the fitted parameters are very poorly determined.

For comparison, Table 6 shows corresponding fit results using $\mathcal{O}(\alpha_s^2)$ QCD. The dependence of α_s and χ^2/d.o.f. on x_μ is shown in Fig. 5. Generally the $\mathcal{O}(\alpha_s^2)$ calculations give a significantly better χ^2 when a value $x_\mu \ll 1$ is adopted, the only exception being B_T. This strong scale dependence is an indication of substantial missing higher order contributions. Comparing with the NLLA fit results in Table 5 we note that in several cases the inclusion of the NLLA terms in the QCD calculation improves the fit to the data for $x_\mu = 1$. However, the $\mathcal{O}(\alpha_s^2)$ fits with optimised scale generally yield values of χ^2/d.o.f. as good as those obtained from the NLLA calculations. The most striking aspect of the NLLA fits is the elimination of the preference for very small x_μ values.

In Table 7 we show the effect of using different matching schemes to combine the NLLA and $\mathcal{O}(\alpha_s^2)$ calculations. As discussed above, and in Ref. [23], the R-matching scheme is theoretically less favoured, since it fails to exponentiate some terms which are exponentiated in the $\ln(R)$- or modified R-schemes. The fits to the data are poor in the R-scheme for B_W and B_T (for which the coefficient G_{21} is particularly large), and to a lesser extent for M_H, R_2 and $\mathcal{N}$. The modified R-scheme, in which the deficiencies of the naïve R-scheme are remedied by exponentiating the G_{21} term, yields results which are very close to the $\ln(R)$-scheme. The modified $\ln(R)$-scheme, in which correct behaviour of the NLLA calculations is enforced near the kinematic limit, gives a significantly improved fit to the data for M_H, B_T, and particularly B_W, though the value of α_s is scarcely affected. We therefore use the $\ln(R)$-matching scheme to obtain our standard results throughout this analysis, except for Σ_{EEC}, where the modified R-scheme is used instead.

4.3 Estimation of Systematic Uncertainties

The values of $\alpha_s(M_{Z^0})$ for the seven observables together with their statistical errors are given in Table 8. Before a meaningful value of α_s can be quoted it is necessary to investigate various possible sources of systematic uncertainty. With the present amount of data these systematic effects prove totally to dominate the small statistical errors. The systematic effects may be grouped under the following headings:

4.3.1 Experimental uncertainties

The corrections for detector acceptance and resolution depend upon the Monte Carlo simulation giving a faithful description of the real data. In our standard analysis both measured tracks and electromagnetic energy clusters were used. The analysis was repeated using tracks alone or the electromagnetic calorimetry alone, thus yielding samples of corrected data with completely independent detector corrections. The analysis was also repeated with several independent modifications to the event selection criteria: firstly restricting the thrust axis to lie within the barrel region of the detector ($|\cos\theta| < 0.7$), secondly increasing the minimum track multiplicity cut to 7 to eliminate background more securely, and finally using a cut on missing momentum ($|\boldsymbol{p}_{vis}|/E_{vis} < 0.4$), where $\boldsymbol{p}_{vis}$ is the vector sum of all the detected particle momenta. Values of α_s were computed from each of these alternative analyses and the largest difference between any pair was assigned as a systematic error. In all cases this proved to result from the difference between tracks alone and electromagnetic calorimetry alone. The systematic error derived for each observable is given in Table 8.

4.3.2 Hadronization uncertainties

Since the NLLA QCD calculations are based on the leading logarithm approximation it is most appropriate to correct for hadronization effects using parton shower QCD Monte Carlo models which are based on essentially the same approximation. However, this correction is far from unambiguous, since the parton shower Monte Carlo models incorporate mass effects and cutoffs in ways which are different from the analytic NLLA calculations. Furthermore different models are available for the hadronization process, which involve many free parameters determined from fits to data.

We have considered several different models for the hadronization correction, retaining the standard detector corrections based on the full simulation of the OPAL detector using JETSET 7.3. The resulting changes in α_s for each observable are given in Table 8. The following have been investigated:

- Some of the parameters of the JETSET 7.3 model [43] were determined from a fit to OPAL data on global event shapes [42]. This fit procedure yielded values of the parameters with some range of uncertainty, so we have independently varied the two parameters which are specifically related to hadronization, σ_q=`PARJ(21)`$=0.37^{+0.03}_{-0.05}$ GeV and a=`PARJ(41)`$=0.18^{+0.12}_{-0.05}$, by ± 1 standard deviation about their optimized values. The effect of these changes was generally found to be modest.

- The OPAL standard version of JETSET uses the Lund symmetric fragmentation model. An alternative which is favoured for many heavy flavour studies is the form proposed by Peterson et al. [49], which is available as an option in JETSET. We have therefore tried using an alternative set of fragmentation parameters [45], again derived by fitting OPAL data, in which

the Peterson form is used for heavy flavour fragmentation. The effect on the fitted α_s value is small.

- The analytic QCD calculations assume the partons are massless, and therefore predict the same distributions for any quark flavour. The parton shower Monte Carlo programs assign masses to the quarks, and indeed the parton level distributions exhibit some differences between heavy and light quarks for the observables considered here. We have therefore, in JETSET 7.3, investigated the effect of performing the hadronization correction by excluding $\mathrm{b\overline{b}}$ events at the parton level, whilst including all flavours at the hadron level. In this way the corrected parton level distribution corresponds to u,d,s,c quarks only. The resulting value of α_s was found to be systematically larger (by about 0.002 on average) for all observables.

- The parton shower Monte Carlo programs incorporate a minimum value, Q_0, for the parton virtuality; for example $Q_0 = 1$ GeV in JETSET 7.3 with the OPAL parameter set. In contrast the NLLA calculations impose no such cutoff. We have therefore tried varying the value of Q_0 in JETSET between 4 GeV and the mimimum value permitted ($Q_0 = 2.2 \times \Lambda = 0.638$ GeV). We find that, within this range, the value of α_s derived from the data varies approximately linearly with the value of Q_0 used in the hadronization correction. We therefore take the difference between the values of α_s corresponding to $Q_0 = 1$ GeV and $Q_0 = 2$ GeV as a (symmetric) systematic error resulting from this source; insofar as the linear approximation is valid this would encompass the value $Q_0 = 0$. As seen from Table 8, the value of α_s is not strongly dependent on Q_0.

- The HERWIG program [44] uses a cluster fragmentation model which is quite different from the string model [50] employed in JETSET. We have used version 5.5 of HERWIG, with parameters based on a tuning to OPAL event shape data [45]. In several cases, this constitutes the largest hadronization uncertainty in α_s, though the effect is not in the same direction for all observables.

- The ARIADNE model [51] uses a colour dipole formulation of the parton shower, with the standard Lund string model for hadronization. We used ARIADNE version 3.1 with parameters tuned to OPAL data [42]; in most cases the influence on α_s is small.

- The COJETS model [52] uses an incoherent parton shower with independent fragmentation. We used version 6.23 with default parameters. However, the parton shower in this model does not evolve so far as in the other models considered (the average number of partons is 3.3, compared to 9.1 in JETSET). It therefore appears that COJETS, with its present parameters, is not appropriate at the parton level for comparison with the NLLA calculations, which implicitly incorporate multi-parton final states. For this reason, and for other reasons outlined in Ref. [5], we exclude COJETS from the final assignment of systematic errors, though we show the effect of using it in Table 8.

It is arguable that the hadronization effects listed above are not altogether independent (for example, JETSET and HERWIG use different effective cutoffs in the parton shower). However, none of the models is likely to be perfect, so in order not to underestimate this uncertainty we define a total hadronization error for each observable by adding in quadrature the following: the larger of the changes in α_s when a is changed by $+1$ and -1 standard deviation, the larger of the changes in α_s when σ_q is changed by $+1$ and -1 standard deviation, the change in α_s when only u,d,s,c quarks are considered in JETSET, the change in α_s when Peterson fragmentation is used in JETSET, the change in α_s when $Q_0 = 2$ GeV is used in JETSET, the change in α_s when HERWIG is used and the change in α_s when ARIADNE is used. This total error is given in Table 8. It appears that the single hemisphere variables, B_W and M_H, are the least sensitive to hadronization, while B_T is the most sensitive of the observables considered here.

4.3.3 Renormalization scale uncertainties

The choice of the value of x_μ is a significant source of systematic uncertainty, but the precise way to quantify this error is essentially arbitrary. This uncertainty is generally understood to be connected with higher order contributions missing from the QCD calculations. In our previous $\mathcal{O}(\alpha_s^2)$ analysis [5] we discussed various procedures to define x_μ, but finally chose to average the values of $\alpha_s(M_{\mathrm{Z}^0})$ obtained with $x_\mu = 1$ and with x_μ fitted to data, and to quote half their difference as a systematic error. However, this procedure does not seem appropriate for the present NLLA+$\mathcal{O}(\alpha_s^2)$ analysis. In some cases the optimal fitted value of x_μ is close to 1, in which case the previous method would underestimate the scale uncertainty. Furthermore, in some cases χ^2 does not show a well defined minimum, falling slowly but monotonically with increasing x_μ. We therefore choose to define the scale uncertainty to be the variation in $\alpha_s(M_{\mathrm{Z}^0})$ as the renormalization scale factor is varied in the range $0.5 < x_\mu < 2$. The case $x_\mu = 1$ is taken to be the central value, so the scale error is asymmetric in general.

4.3.4 Matching scheme uncertainties

Different matching schemes were discussed in Sect. 4.1; they are equivalent so far as the leading and next-to-leading terms are concerned, but differ in the higher order terms generated by exponentiation. Therefore the differences between the results in Table 7 represent a further measure of possible higher order effects. In those cases where more than two matching schemes were available, we observe that all the matching procedures except for the R-scheme yield very similar values of α_s. Since the R-scheme is disfavoured both theoretically, and in many cases by the χ^2/d.o.f. values of the fits, we choose to discount it. The remaining uncertainty in α_s resulting from different matching procedures is much smaller than the error already assigned on the basis of x_μ dependence. Since the two effects may be expected to be correlated because both relate to missing higher orders, we assign no additional error resulting from the choice of matching scheme.

4.3.5 Explicit inclusion of subleading logarithms

As a final check of possible higher order effects, we have investigated the possibility of including a subleading logarithmic term in the fit. In the case of $(1-T)$, M_H, B_T, B_W and Σ_{EEC}, and for all matching schemes except R-matching, the leading and next-to-leading logarithms and the subleading term $G_{21}\overline{\alpha}_s^2 L$ are all resummed, and hence the first subleading logarithmic term to be absent from the resummation is $G_{32}\overline{\alpha}_s{}^3 L^2$. We have therefore performed fits to the data including a term of this form in the exponentiation, treating G_{32} as a free parameter to be determined in the fit. The results are summarized in Table 9. The values of χ^2/d.o.f. are substantially improved by the inclusion of the subleading term, suggesting that higher order effects might in large part account for the values of χ^2/d.o.f. in the standard analysis being greater than unity. The fitted values of G_{32} are different for different matching schemes, indicating that this term is effectively parametrizing a mixture of higher order terms. Naïvely one might guess that the values of G_{32} could be greater than G_{21} by a factor of order 2π (since a factor $(2\pi)^{-1}$ appears in $\overline{\alpha}_s$), and the fitted values are therefore not of unreasonable size. By reference to Table 5, we note that varying G_{32} in the fits yields better χ^2/d.o.f. values than varying x_μ. Also the values of α_s for the different variables tend to move slightly closer together when G_{32} is fitted, in contrast to their behaviour when x_μ is fitted. The most important feature is that the changes in the fitted values of α_s when G_{32} is fitted are small, and contained within the errors already assigned from the study of x_μ dependence. We therefore assign no additional sytematic error as a result of this study.

4.3.6 Final errors on $\alpha_s(M_{Z^0})$

Finally, the statistical error, the experimental systematic uncertainty, the hadronization error, and the scale uncertainty are all combined in quadrature to yield the errors given in the final row of Table 8. The values are also shown in Fig. 6. If only experimental errors are taken into account, the results (in particular those from B_W and Σ_{EEC}) are not compatible with a common value, especially if correlations between the systematic contributions are taken into consideration. If the full systematic errors are considered then there appears to be no inconsistency, but again the observables are not fully independent, as discussed below.

4.4 Combined Result

A particular emphasis of this analysis was to study all the observables for which resummed QCD calculations are available. It is therefore instructive to combine the measurements of α_s from the seven variables considered in this analysis, in order to assess the degree of consistency with which QCD describes the data, and in order to arrive at a "best estimate" of $\alpha_s(M_{Z^0})$. We have considered three methods:

4.4.1 Weighted Mean

This method is essentially identical to that employed in the previous OPAL paper [5]. A weighted mean was formed:

$$\widehat{\alpha}_s = \sum_{i=1}^{7} w_i {\alpha_s}^{(i)} / \sum_{i=1}^{7} w_i$$

where ${\alpha_s}^{(i)}$ is the value of α_s derived from the i^{th} observable, and the weight w_i is equal to the reciprocal of the square of the total error on ${\alpha_s}^{(i)}$ as given in Table 8. In order to estimate the error on the weighted mean statistical correlations between the different observables were ignored, but correlations in the systematic uncertainties were taken into account by forming the mean $\widehat{\alpha}_s$ of the values obtained in each of the different systematic checks described in Sect. 4.3. A systematic uncertainty on $\widehat{\alpha}_s$ was then derived from the different mean values following the same procedure as for the individual ${\alpha_s}^{(i)}$ measurements.

Applying this procedure to all seven observables we obtain the value:

$$\alpha_s(M_{Z^0}) = 0.120 \pm 0.003 \text{ (expt.)} \; {}^{+0.006}_{-0.004} \text{ (theor.)}$$

where the first error includes statistical and experimental systematic effects, while the second includes the hadronization and scale uncertainties. If the B_W variable, which gave a rather low value of α_s and also the smallest overall error, were excluded the mean would increase to 0.123, if Σ_{EEC} were excluded the mean would be 0.118, while if both were removed the mean would be 0.121. The NLLA calculations are arguably less reliable for Σ_{EEC} (an unphysical pole is introduced in the calculation, though well outside the fit region) and for the jet rates (the next-to-leading resummation is incomplete); if we were to average the other observables, $(1-T)$, M_H, B_T and B_W, we would obtain 0.116. Thus the overall mean of all seven observables yields a value and an error which comfortably encompasses the mean of any reasonable subset.

4.4.2 Minimization of χ^2

In order to account for the correlation between observables in a more formal way, we have estimated the value $\widehat{\alpha}_s$ which is most consistent with all the measurements, by minimizing

$$\chi^2 = \sum_{i=1}^{7}\sum_{j=1}^{7}(\widehat{\alpha}_s - {\alpha_s}^{(i)})(\mathcal{V}^{-1})_{ij}(\widehat{\alpha}_s - {\alpha_s}^{(j)})$$

with respect to $\widehat{\alpha}_s$, where $\mathcal{V}$ is the covariance matrix of the seven individual measurements. The statistical part of $\mathcal{V}$ was estimated by dividing the data and Monte Carlo samples into ten subsamples, determining values of ${\alpha_s}^{(i)}$ from each, and measuring the covariances between them. To this was added a matrix associated with each of the detector and hadronization systematic effects listed in Sect. 4.3[‖]. Following this procedure for the case x_μ=1 we find an unacceptable value of χ^2/d.o.f.=34, with a value of $\widehat{\alpha}_s$=0.113 which lies below most of the measurements on account of strong positive correlations between the systematic errors. The large value of χ^2/d.o.f. is associated with Σ_{EEC}, and to a lesser extent B_W; restricting the procedure to the other five observables we could obtain χ^2/d.o.f.=0.3 and $\widehat{\alpha}_s$=0.121, showing that these five are very compatible.

Thus the NLLA+$\mathcal{O}(\alpha_s^2)$ theory appears to be unable to describe Σ_{EEC} and B_W simultaneously with the other five variables, if the systematic errors and their correlations are estimated as described above, and if the value of x_μ is fixed to the same value for all observables. However, if the scale error given in Table 8 is included in the diagonal terms of $\mathcal{V}$ then a satisfactory value of χ^2/d.o.f.=1.7 may be obtained using all seven observables, with $\widehat{\alpha}_s = 0.119 \pm 0.004$, in agreement with the weighted mean in Sect. 4.4.1. This procedure effectively allows the α_s value corresponding to each observable to vary independently by an amount corresponding to the range $0.5 < x_\mu < 2$. However, it does not address the extent to which the χ^2/d.o.f. of the fit to the data depends on x_μ; this is considered in the next section.

4.4.3 Combined fit

In a previous OPAL paper [5] we introduced a method for investigating the consistency of QCD by performing a simultaneous fit to the distributions of many observables using a common value of $\Lambda_{\overline{MS}}$. In the case of $\mathcal{O}(\alpha_s^2)$ QCD we found that such a simultaneous fit could be successful, but only if the renormalization scale factor, x_μ, was allowed to vary independently for each observable, most of the fitted values of x_μ being much smaller than unity.

Accordingly we have attempted a similar fit of NLLA+$\mathcal{O}(\alpha_s^2)$ QCD to the present data. The same fit ranges were used as for the standard fits, but in order that each observable carry equal weight in the fit, bins in the data were combined so as to form an equal number of bins, seven for each observable. Correlations between the errors on different observables were neglected. As usual, the ln(R)-matching scheme was used except for Σ_{EEC}, where the modified R-scheme was taken. The result of a combined fit to all seven observables with $x_\mu = 1$ was α_s=0.122, in good agreement with the weighted mean described in Sect. 4.4.1. However, the combined fit gave an unacceptable value of χ^2/d.o.f.=93, some ten times greater than expected from the sum of the χ^2 values of the separate fits. This large value of χ^2 was mainly contributed by the Σ_{EEC} and B_W variables; if these two were removed a combined fit to the remaining five variables yielded α_s=0.121 with χ^2/d.o.f.=8.8. The procedure of allowing the x_μ

[‖]If the change in ${\alpha_s}^{(i)}$ resulting from a particular systematic check was $\delta{\alpha_s}^{(i)}$ then $\delta{\alpha_s}^{(i)}\delta{\alpha_s}^{(j)}$ was added to the element $\mathcal{V}_{ij}$ of the covariance matrix. This corresponds to assuming correlation coefficients of ± 1 in the error matrix associated with each individual effect.

values to vary is not so obviously reasonable in the NLLA case as in the $\mathcal{O}(\alpha_s^2)$ analysis. Nevertheless, if such a fit is performed, an acceptable χ^2 may be achieved with all seven observables, but with a large value α_s=0.143 and $x_\mu \gg 1$ for all observables. This seems to be needed in order to accommodate Σ_{EEC}, where a reduction of α_s to around 0.120 would lead to a large increase in χ^2/d.o.f.. A fit to the remaining six observables with x_μ free gives α_s=0.121, with χ^2/d.o.f.=7.7 and all x_μ values in the vicinity of unity. Alternatively, a fit to all seven observables, but using the R-matching scheme for Σ_{EEC} yields α_s=0.124 with χ^2/d.o.f.=7.9 and x_μ values close to unity. Similar results may be obtained from a combined fit (excluding R_2 and $\mathcal{N}$) in which x_μ is fixed to 1 while the subleading coefficient G_{32} is allowed to vary independently for each observable.

Thus, these combined fits indicate that, given the presently available calculations, Σ_{EEC}, and to a lesser extent B_W, cannot be described by NLLA+$\mathcal{O}(\alpha_s^2)$ QCD simultaneously with the other observables, particularly if x_μ=1 is assumed. Nonetheless, an average value of $\alpha_s(M_{Z^0})$ around 0.120 seems quite reliable.

5 Discussion and Summary

Resummed QCD calculations have been introduced in an attempt to describe the two-jet region in e^+e^- hadronic final states. In this region the previously available $\mathcal{O}(\alpha_s^2)$ QCD matrix elements were clearly insufficient because of the presence of large logarithms connected with soft and collinear singularities. Resummed calculations are now available for seven observables, which we have studied in this analysis. Two of the observables, B_T and B_W, had not been studied in e^+e^-annihilation before the calculations were performed, and therefore constitute a new test of the theory. Although jet rates have been extensively studied before, the Durham jet finder is comparatively new and measurements for R_2 and $\mathcal{N}$ were not available before the calculations. The calculations should be most secure for $(1-T)$, M_H, B_T and B_W, for which complete resummation of leading and next-to-leading logarithms was done. For the jet rates only part of the next-to-leading logarithms were resummed, while the analytic solution of the Σ_{EEC} calculation in Ref. [24] introduced an unphysical pole which limits the region of applicability of the theory.

Comparison of the theory with data in Figs. 2 and 3 shows that a good qualitative description of the data in the two-jet region is obtained. However, in this region the corrections which relate the observed hadron level to the parton level where the QCD calculations are relevant are, at present energies, large and subject to significant uncertainties. We have therefore chosen to combine the NLLA and $\mathcal{O}(\alpha_s^2)$ calculations, and fit to data in the region where the hadronization corrections are reasonably small and reliable. However, in the more extreme hard region the higher order contributions which are absent from the $\mathcal{O}(\alpha_s^2)$ theory are not necessarily dominated by the leading logarithms which we include in the present approach, and the leading logarithmic terms could even have an opposite sign from the uncomputed higher orders. Thus in this region the inclusion of the NLLA terms could even degrade the description of data, as seen particularly for M_H and B_W in Fig. 2.

The NLLA+$\mathcal{O}(\alpha_s^2)$ QCD calculations, with renormalization scale factor x_μ=1, were found to give reasonable fits to the OPAL data. In some cases the fits were better than those obtained using $\mathcal{O}(\alpha_s^2)$ QCD alone with x_μ=1, though no better than $\mathcal{O}(\alpha_s^2)$ fits with optimized scale. However, the $\mathcal{O}(\alpha_s^2)$ fits where x_μ was optimized generally yielded values $x_\mu < 0.1$, whilst such low values of $x_\mu$were clearly disfavoured by the NLLA+$\mathcal{O}(\alpha_s^2)$ calculations. The dependence of $\alpha_s(M_{Z^0})$ on the choice of x_μ was slightly weaker when the resummed theory was included, but still remained the principal source of systematic uncertainty.

Table 10 shows the final results for $\alpha_s(M_{Z^0})$ obtained from each of the seven observables using NLLA+$\mathcal{O}(\alpha_s^2)$ QCD, with the corresponding results obtained from the same data using $\mathcal{O}(\alpha_s^2)$ QCD alone for comparison. The experimental errors were essentially the same for both approaches, and the same as in our previous publication [5]. The hadronization uncertainties were estimated in the same way for both sets of measurements, though a larger range of hadronization models was considered than in our previous paper [5]. As in our previous work a wider variation of $1 < Q_0 < 6$ GeV was considered for the $\mathcal{O}(\alpha_s^2)$ analysis. The principal difference between the NLLA and $\mathcal{O}(\alpha_s^2)$ analyses was however the treatment of the renormalization scale uncertainty; in the NLLA+$\mathcal{O}(\alpha_s^2)$ case we took x_μ=1 as the central value, assigning an error by considering the range $0.5 < x_\mu < 2$, while in the $\mathcal{O}(\alpha_s^2)$ analysis we followed our procedure in Ref. [5], taking the central value to be the mean of the values of $\alpha_s(M_{Z^0})$ from x_μ=1 and x_μ fitted, and quoting half their difference as the error. Figures 6 and 7 show the values of α_s so obtained, together with their weighted means.

Neither the $\mathcal{O}(\alpha_s^2)$ nor the NLLA+$\mathcal{O}(\alpha_s^2)$ calculations give a consistent description of the data with x_μ=1 if only experimental errors are taken into account. After making due allowance for systematic uncertainties the $\mathcal{O}(\alpha_s^2)$ measurements are compatible with a common mean value of 0.122 ± 0.007. These conclusions are consistent with our previous study of thirteen observables to $\mathcal{O}(\alpha_s^2)$ [5], only three of which (T, M_H and R_2) are shared with the present study. The value obtained here is very close to that obtained in Ref. [5], $0.122^{+0.006}_{-0.005}$. When the systematic uncertainties are taken into account in the NLLA+$\mathcal{O}(\alpha_s^2)$ analysis, we find that the individual measurements are compatible with a common mean of 0.120 ± 0.006, which is in excellent agreement with the $\mathcal{O}(\alpha_s^2)$ analysis. However, because the systematic uncertainties are correlated it is not clear that the values of α_s obtained from the B_W and Σ_{EEC} variables are really compatible with this value. The case of B_W is somewhat disappointing, since this variable has the smallest overall error, with a particularly weak hadronization uncertainty. Nonetheless, the values derived from B_W and Σ_{EEC} lie within two standard deviations of the weighted mean, which therefore seems a reasonable estimate of α_s. In the $\mathcal{O}(\alpha_s^2)$ analysis the B_W and Σ_{EEC} observables exhibit no anomalous behaviour.

In previous measurements of α_s based on $\mathcal{O}(\alpha_s^2)$ QCD the main uncertainty was the effect of missing higher order terms, manifested particularly in the renormalization scale dependence. In the present study the NLLA calculations have been used to supplement the $\mathcal{O}(\alpha_s^2)$ theory with some higher order information. However, the NLLA+$\mathcal{O}(\alpha_s^2)$ calculations have not brought about a dramatic reduction in the error on α_s. This is partly because the observables which showed the smallest scale dependence in $\mathcal{O}(\alpha_s^2)$ (such as the asymmetry in the EEC or the jet mass difference) have not so far proved amenable to resummation. Nevertheless, the inclusion of the NLLA terms has removed the need to consider very small renormalization scales; indeed the data are incompatible with such scales. After investigating several ways to combine the measurements of α_s we quote as our final result that based on a simple weighted average:

$$\alpha_s(M_{Z^0}) = 0.120 \pm 0.006 \quad .$$

The error is competitive with, but marginally larger than that obtained in our previous $\mathcal{O}(\alpha_s^2)$ measurement [5]. It also agrees well with the NLLA+$\mathcal{O}(\alpha_s^2)$ measurement in Ref. [5], and with other measurements of α_s at LEP and elsewhere, summarized in Ref. [18]. The error is however slightly smaller than that resulting from an $\mathcal{O}(\alpha_s^2)$ analysis performed on the present data. This new result based on NLLA+$\mathcal{O}(\alpha_s^2)$ QCD is therefore an important measurement, complementary to those obtained from $\mathcal{O}(\alpha_s^2)$ QCD; the fact that they are in such good agreement gives us confidence that higher order uncertainties are under control at the level of the errors which we quote.

Acknowledgements

We thank S. Catani, G. Turnock and B.R. Webber for many enlightening discussions and useful suggestions concerning parts of this analysis.

It is a pleasure to thank the SL Division for the efficient operation of the LEP accelerator, the precise information on the absolute energy, and their continuing close cooperation with our experimental group. In addition to the support staff at our own institutions we are pleased to acknowledge the
Department of Energy, USA,
National Science Foundation, USA,
Texas National Research Laboratory Commission, USA,
Science and Engineering Research Council, UK,
Natural Sciences and Engineering Research Council, Canada,
Fussefeld Foundation,
Israeli Ministry of Energy,
Israeli Ministry of Science,
Minerva Gesellschaft,
Japanese Ministry of Education, Science and Culture (the Monbusho) and a grant under the Monbusho International Science Research Program,
German Israeli Bi-national Science Foundation (GIF),
Direction des Sciences de la Matière du Commissariat à l'Energie Atomique, France,
Bundesministerium für Forschung und Technologie, FRG,
National Research Council of Canada, Canada,
A.P. Sloan Foundation and Junta Nacional de Investigação Científica e Tecnológica, Portugal.

References

[1] H. Fritzsch, M. Gell-Mann, 16^{th} Int. Conf. on High Energy Physics, Chicago (1972);
H. Fritzsch, M. Gell-Mann and H. Leutwyler, Phys. Lett. **B47** (1973) 365;
D. Gross and F. Wilczek, Phys. Rev. Lett. **30** (1973) 1343;
H.D. Politzer, Phys. Rev. Lett. **30** (1973) 1346.

[2] U. Amaldi, W. de Boer and H. Fürstenau, Phys. Lett. **B260** (1991) 447;
U. Amaldi et al., Phys. Lett. **B281** (1992) 374;
F. Anselmo, L. Cifarelli, A. Petermann and A. Zichichi, Nuov. Cim. **104A** (1991) 1817;
J. Ellis, S. Kelley and D.V. Nanopoulos, Nucl. Phys. **B373** (1992) 55.

[3] R.K. Ellis, D.A. Ross and A.E. Terrano, Nucl. Phys. **B178** (1981) 421.

[4] Z.Kunszt and P.Nason [conv.], in "Z Physics at LEP 1" (eds. G.Altarelli, R.Kleiss and C.Verzegnassi), CERN 89-08 (1989).

[5] Opal Collaboration, P.D. Acton et al., Z. Phys. **C55** (1992) 1.

[6] Opal Collaboration, M.Z. Akrawy et al., Phys. Lett. **B235** (1991) 389.

[7] Opal Collaboration, M.Z. Akrawy et al., Z. Phys. **C49** (1991) 375.

[8] Opal Collaboration, M.Z. Akrawy et al., Phys. Lett. **B252** (1990) 159.

[9] Opal Collaboration, P.D. Acton et al., Phys. Lett. **B276** (1992) 547.

[10] ALEPH Collaboration, D. Decamp et al., Phys. Lett. **B255** (1991) 623.

[11] ALEPH Collaboration, D. Decamp et al., Phys. Lett. **B257** (1991) 479.

[12] DELPHI Collaboration, P. Abreu et al., Phys. Lett. **B247** (1990) 167.

[13] DELPHI Collaboration, P. Abreu et al., Phys. Lett. **B252** (1990) 149.

[14] DELPHI Collaboration, P. Abreu et al., Z. Phys. **C54** (1992) 55.

[15] L3 Collaboration, B. Adeva et al., Phys. Lett. **B248** (1991) 464.

[16] L3 Collaboration, B. Adeva et al., Phys. Lett. **B257** (1991) 469.

[17] L3 Collaboration, B. Adeva et al., Phys. Lett. **B271** (1991) 461.

[18] S. Bethke, Preprint HD-PY-92-13, Proc. XXVI Int. Conf. on High Energy Physics, Dallas, August 1992.

[19] L. Rolandi, Preprint CERN-PPE/92-175, Proc. XXVI Int. Conf. on High Energy Physics, Dallas, August 1992.

[20] S. Catani, L. Trentadue, G. Turnock and B.R. Webber, Phys. Lett. **B263** (1991) 491.

[21] S. Catani, L. Trentadue, G. Turnock and B.R. Webber, Preprint CERN-TH.6640/92.

[22] S. Catani, G. Turnock and B.R. Webber, Phys. Lett. **B272** (1991) 368.

[23] S. Catani, G. Turnock and B.R. Webber, Phys. Lett. **B295** (1992) 269.

[24] G. Turnock, Cambridge Preprint Cavendish-HEP-92/3; Ph. D. Thesis, University of Cambridge (1992).

[25] J.C. Collins and D.E. Soper, Nucl. Phys. **B193** (1981) 381;
J.C. Collins and D.E. Soper, Nucl. Phys. **B197** (1982) 446; erratum Nucl. Phys. **B213** (1983) 545;
J.C. Collins and D.E. Soper, Nucl. Phys. **B284** (1987) 253;
J. Kodaira and L. Trentadue, Phys. Lett. **B112** (1982) 66;
R. Fiore, A. Quartarolo and L. Trentadue, Phys. Lett. **B294** (1992) 431.

[26] S. Catani, Yu.L. Dokshitzer, M. Olsson, G. Turnock and B.R. Webber, Phys. Lett. **B269** (1991) 432.

[27] S. Catani, Yu.L. Dokshitzer, F. Fiorani and B.R. Webber, Nucl. Phys. **B377** (1992) 445.

[28] ALEPH Collaboration, D. Decamp et al., Phys. Lett. **B284** (1992) 163.

[29] L3 Collaboration, O. Adriani et al., Phys. Lett. **B284** (1992) 471.

[30] DELPHI Collaboration, contributed paper at the XXVI Int. Conf. on High Energy Physics, Dallas, August 1992;
J. Chrin and J. Fuster, Preprint CERN-PPE/92-201.

[31] OPAL Collaboration, K. Ahmet et al., Nucl. Instr. and Meth. **A305** (1991) 275.

[32] M. Arignon et al., Nucl. Instr. and Meth. **A313** (1992) 103.

[33] D.G. Charlton, F. Meijers, T.J. Smith and P.S. Wells, Nucl. Instr. and Meth. **A325** (1993) 129.

[34] OPAL Collaboration, G. Alexander et al., Z. Phys. **C52** (1991) 175.

[35] S. Brandt et al., Phys. Lett. **12** (1964) 57;
E. Farhi, Phys. Rev. Lett. **39** (1977) 1587.

[36] T. Chandramohan and L. Clavelli, Nucl. Phys. **B184** (1981) 365.

[37] Mark J Collaboration, D.P. Barber et al., Phys. Rev. Lett. **43** (1979) 830;
Mark J Collaboration, D.P. Barber et al., Phys. Lett. **B89** (1979) 139.

[38] C.L. Basham et al., Phys. Rev. Lett. **41** (1978) 1585;
C.L. Basham et al., Phys. Rev. **D17** (1978) 2298.

[39] S. Bethke, Z. Kunszt, D. Soper and W.J. Stirling, Nucl. Phys. **B370** (1992) 310.

[40] N. Brown and W.J. Stirling, Z. Phys. **C53** (1992) 629.

[41] J. Allison et al., Nucl. Instr. and Meth. **A317** (1992) 47.

[42] OPAL Collaboration, M.Z. Akrawy et al., Z. Phys. **C47** (1990) 505.

[43] T. Sjöstrand, Comp. Phys. Commun. **39** (1986) 347;
T. Sjöstrand, Comp. Phys. Commun. **43** (1987) 367;
M. Bengtsson and T. Sjöstrand, Nucl. Phys. **B289** (1987) 810.

[44] G. Marchesini and B.R. Webber, Nucl. Phys. **B310** (1988) 461;
G. Marchesini et al. Comp. Phys. Commun. **67** (1992) 465.

[45] OPAL Collaboration, P.D. Acton et al., CERN-PPE/93-02, submitted to Z. Phys. C.

[46] B.R. Webber, "Jets in Perturbation Theory", Proc. 'QCD – 20 Years later', Aachen (1992), CERN-TH-6706-92.

[47] B.R. Webber, Private Communication.

[48] Particle Data Group, K. Hikasa et al., *Review of Particle Properties*, Phys. Rev. **D45** (1992) 1.

[49] C. Peterson, D. Schlatter, I. Schmitt and P.M. Zerwas, Phys. Rev. **D27** (1983) 105.

[50] B. Andersson, G. Gustafson, G. Ingelman and T. Sjöstrand, Phys. Rep. **97** (1983) 31.

[51] U. Pettersson, LU TP 88-5 (1988);
L. Lönnblad and U. Pettersson, LU TP 88-15 (1988);
L. Lönnblad, LU TP 89-10 (1988).

[52] R. Odorico, Comp. Phys. Commun. **32** (1984) 139;
R. Odorico, Comp. Phys. Commun. **59** (1990) 527.

$(1-T)$	$\frac{1}{\sigma}\frac{d\sigma}{dT}$	$M_H/\sqrt{s}$	$\frac{1}{\sigma}\frac{d\sigma}{d(M_H/\sqrt{s})}$	B_T	$\frac{1}{\sigma}\frac{d\sigma}{dB_T}$	B_W	$\frac{1}{\sigma}\frac{d\sigma}{dB_W}$
0.005	1.36 ± 0.23	0.02	0.009 ± 0.007	0.01	0.028 ± 0.018	0.005	0.04 ± 0.03
0.015	11.81 ± 0.90	0.05	0.075 ± 0.009	0.025	0.31 ± 0.06	0.015	0.96 ± 0.16
0.025	18.42 ± 0.57	0.07	0.182 ± 0.028	0.035	2.28 ± 0.45	0.025	10.33 ± 1.17
0.035	14.38 ± 0.12	0.09	0.915 ± 0.097	0.045	6.83 ± 0.90	0.035	17.20 ± 0.76
0.045	10.03 ± 0.16	0.11	3.10 ± 0.22	0.055	10.49 ± 0.75	0.045	13.65 ± 0.08
0.055	7.33 ± 0.15	0.13	5.88 ± 0.26	0.065	11.26 ± 0.32	0.055	10.36 ± 0.13
0.065	5.62 ± 0.15	0.15	7.00 ± 0.17	0.075	9.98 ± 0.07	0.065	8.31 ± 0.18
0.075	4.57 ± 0.14	0.17	6.19 ± 0.06	0.085	8.46 ± 0.16	0.075	6.70 ± 0.19
0.085	3.76 ± 0.12	0.19	4.88 ± 0.05	0.095	7.06 ± 0.21	0.085	5.46 ± 0.19
0.095	3.14 ± 0.10	0.21	3.87 ± 0.06	0.105	6.02 ± 0.22	0.095	4.56 ± 0.17
0.105	2.64 ± 0.08	0.23	3.19 ± 0.07	0.115	5.17 ± 0.20	0.105	3.84 ± 0.15
0.115	2.22 ± 0.07	0.25	2.66 ± 0.06	0.125	4.46 ± 0.18	0.115	3.23 ± 0.13
0.125	1.90 ± 0.06	0.27	2.25 ± 0.06	0.135	3.83 ± 0.16	0.125	2.73 ± 0.11
0.135	1.67 ± 0.06	0.29	1.87 ± 0.06	0.145	3.34 ± 0.14	0.135	2.31 ± 0.10
0.145	1.44 ± 0.05	0.31	1.58 ± 0.06	0.155	2.94 ± 0.12	0.145	1.97 ± 0.09
0.155	1.26 ± 0.05	0.33	1.32 ± 0.05	0.165	2.51 ± 0.10	0.155	1.65 ± 0.08
0.165	1.12 ± 0.05	0.35	1.09 ± 0.05	0.175	2.23 ± 0.10	0.165	1.40 ± 0.08
0.175	0.979 ± 0.042	0.37	0.92 ± 0.05	0.185	1.99 ± 0.08	0.175	1.18 ± 0.07
0.185	0.872 ± 0.037	0.39	0.77 ± 0.05	0.195	1.70 ± 0.07	0.185	0.99 ± 0.06
0.195	0.781 ± 0.036	0.41	0.60 ± 0.04	0.205	1.52 ± 0.07	0.195	0.83 ± 0.06
0.205	0.672 ± 0.031	0.43	0.490 ± 0.032	0.215	1.32 ± 0.07	0.205	0.67 ± 0.05
0.215	0.599 ± 0.028	0.45	0.384 ± 0.026	0.225	1.13 ± 0.06	0.215	0.53 ± 0.04
0.225	0.550 ± 0.028	0.47	0.307 ± 0.022	0.235	1.00 ± 0.05	0.225	0.439 ± 0.030
0.235	0.471 ± 0.024	0.49	0.223 ± 0.016	0.245	0.84 ± 0.05	0.235	0.344 ± 0.025
0.245	0.413 ± 0.021	0.51	0.154 ± 0.012	0.255	0.75 ± 0.04	0.245	0.244 ± 0.018
0.255	0.373 ± 0.020	0.53	0.094 ± 0.008	0.265	0.641 ± 0.034	0.255	0.157 ± 0.011
0.265	0.346 ± 0.022	0.55	0.052 ± 0.004	0.275	0.546 ± 0.030	0.265	0.094 ± 0.006
0.275	0.300 ± 0.020	0.57	0.019 ± 0.002	0.285	0.459 ± 0.024	0.275	0.039 ± 0.004
0.285	0.250 ± 0.018			0.295	0.364 ± 0.018		
0.295	0.214 ± 0.013			0.305	0.284 ± 0.015		
0.305	0.192 ± 0.014			0.315	0.201 ± 0.015		
0.315	0.150 ± 0.013			0.325	0.152 ± 0.009		
0.325	0.119 ± 0.009			0.335	0.089 ± 0.005		
0.335	0.102 ± 0.010			0.345	0.044 ± 0.003		
0.345	0.068 ± 0.005						

Table 1: Distributions of the variables defined in the text. The data are corrected for the finite acceptance and resolution of the detector and for initial state photon radiation. No corrections for hadronization effects are applied. The errors include statistical and experimental systematic uncertainties, added in quadrature.

χ(deg.)	Σ_{EEC}	χ(deg.)	Σ_{EEC}
0.9	3.24 ± 0.18	90.9	0.076 ± 0.002
2.7	1.30 ± 0.03	92.7	0.076 ± 0.002
4.5	1.38 ± 0.03	94.5	0.076 ± 0.002
6.3	1.197 ± 0.016	96.3	0.078 ± 0.002
8.1	0.974 ± 0.017	98.1	0.078 ± 0.002
9.9	0.796 ± 0.019	99.9	0.079 ± 0.003
11.7	0.661 ± 0.019	101.7	0.080 ± 0.002
13.5	0.553 ± 0.016	103.5	0.082 ± 0.002
15.3	0.461 ± 0.011	105.3	0.083 ± 0.002
17.1	0.390 ± 0.011	107.1	0.085 ± 0.002
18.9	0.334 ± 0.011	108.9	0.087 ± 0.002
20.7	0.289 ± 0.010	110.7	0.089 ± 0.002
22.5	0.255 ± 0.011	112.5	0.091 ± 0.003
24.3	0.227 ± 0.009	114.3	0.094 ± 0.002
26.1	0.206 ± 0.007	116.1	0.096 ± 0.003
27.9	0.188 ± 0.007	117.9	0.099 ± 0.003
29.7	0.174 ± 0.007	119.7	0.102 ± 0.002
31.5	0.161 ± 0.006	121.5	0.107 ± 0.003
33.3	0.150 ± 0.006	123.3	0.110 ± 0.004
35.1	0.141 ± 0.004	125.1	0.116 ± 0.004
36.9	0.133 ± 0.005	126.9	0.121 ± 0.004
38.7	0.127 ± 0.004	128.7	0.125 ± 0.003
40.5	0.121 ± 0.004	130.5	0.131 ± 0.003
42.3	0.116 ± 0.004	132.3	0.138 ± 0.003
44.1	0.110 ± 0.003	134.1	0.146 ± 0.003
45.9	0.106 ± 0.003	135.9	0.155 ± 0.004
47.7	0.102 ± 0.003	137.7	0.164 ± 0.004
49.5	0.099 ± 0.002	139.5	0.174 ± 0.003
51.3	0.096 ± 0.003	141.3	0.186 ± 0.003
53.1	0.093 ± 0.002	143.1	0.200 ± 0.004
54.9	0.091 ± 0.003	144.9	0.213 ± 0.002
56.7	0.089 ± 0.002	146.7	0.230 ± 0.002
58.5	0.087 ± 0.002	148.5	0.250 ± 0.003
60.3	0.085 ± 0.003	150.3	0.272 ± 0.004
62.1	0.083 ± 0.003	152.1	0.299 ± 0.003
63.9	0.081 ± 0.003	153.9	0.329 ± 0.005
65.7	0.081 ± 0.003	155.7	0.365 ± 0.005
67.5	0.079 ± 0.003	157.5	0.410 ± 0.005
69.3	0.078 ± 0.002	159.3	0.457 ± 0.009
71.1	0.077 ± 0.002	161.1	0.521 ± 0.006
72.9	0.076 ± 0.002	162.9	0.595 ± 0.010
74.7	0.076 ± 0.002	164.7	0.682 ± 0.012
76.5	0.075 ± 0.002	166.5	0.783 ± 0.007
78.3	0.075 ± 0.002	168.3	0.906 ± 0.008
80.1	0.075 ± 0.002	170.1	1.049 ± 0.014
81.9	0.075 ± 0.002	171.9	1.19 ± 0.02
83.7	0.074 ± 0.002	173.7	1.31 ± 0.02
85.5	0.074 ± 0.002	175.5	1.34 ± 0.04
87.3	0.074 ± 0.001	177.3	1.12 ± 0.04
89.1	0.075 ± 0.002	179.1	0.46 ± 0.02

y_{cut}	$\mathcal{N}$
0.0001	8.60±0.24
0.0002	6.76±0.17
0.0007	4.36±0.10
0.001	3.87±0.07
0.002	3.16 ±0.05
0.005	2.63 ±0.03
0.007	2.51 ±0.02
0.01	2.41 ±0.02
0.02	2.258±0.013
0.03	2.188±0.009
0.04	2.147±0.008
0.05	2.118±0.007
0.06	2.098±0.006
0.07	2.083±0.006
0.08	2.070±0.004
0.10	2.051±0.003
0.12	2.038±0.002
0.14	2.028±0.002
0.17	2.018±0.002
0.20	2.011±0.001

y_{cut}	D_2
0.001–0.002	161. ± 10.
0.002–0.005	73.6 ± 0.6
0.005–0.010	26.7 ± 1.4
0.01–0.02	11.5 ± 0.6
0.02–0.03	5.9 ± 0.4
0.03–0.04	3.74 ± 0.19
0.04–0.05	2.64 ± 0.09
0.05–0.06	1.93 ± 0.10
0.06–0.08	1.37 ± 0.08
0.08–0.10	0.93 ± 0.05
0.10–0.12	0.63 ± 0.04
0.12–0.14	0.47 ± 0.03
0.14–0.17	0.33 ± 0.02
0.17–0.20	0.23 ± 0.03

Table 1: (contd.)

	Leading logs	Next-to-Leading logs	Subleading logs	Non-logarithmic terms	
$\ln R(y) =$	$G_{12}\overline{\alpha}_s L^2$	$+ G_{11}\overline{\alpha}_s L$		$+ \alpha_s \mathcal{O}(1)$	$= \mathcal{A}(y)\overline{\alpha}_s$
	$+ G_{23}\overline{\alpha}_s{}^2 L^3$	$+ G_{22}\overline{\alpha}_s{}^2 L^2$	$+ G_{21}\overline{\alpha}_s{}^2 L$	$+ \alpha_s{}^2 \mathcal{O}(1)$	$= (\mathcal{B}(y) - \frac{1}{2}\mathcal{A}(y)^2)\overline{\alpha}_s{}^2$
	$+ G_{34}\overline{\alpha}_s{}^3 L^4$	$+ G_{33}\overline{\alpha}_s{}^3 L^3$	$+ G_{32}\overline{\alpha}_s{}^3 L^2 + \cdots$	$+ \cdots$	$\mathcal{O}(\alpha_s{}^3)$
	$+ G_{45}\overline{\alpha}_s{}^4 L^5$	$+ G_{44}\overline{\alpha}_s{}^4 L^4$	$+ G_{43}\overline{\alpha}_s{}^4 L^3 + \cdots$	$+ \cdots$	$\mathcal{O}(\alpha_s{}^4)$
	$+ \cdots$	$+ \cdots$	$+ \cdots$	$+ \cdots$	
$=$	$L g_1(\alpha_s L)$	$+ g_2(\alpha_s L)$	$+ \cdots$	$+ \cdots$	

Table 2: Decomposition of the cumulative cross-section, $\ln R(y)$, in powers of $\overline{\alpha}_s = (\alpha_s/2\pi)$ and $L = \ln(1/y)$. The NLLA calculations provide the terms in the first two columns, while the $\mathcal{O}(\alpha_s^2)$ calculations yield the sums of the terms in the first two rows. The matching procedures involve combining these without double-counting the terms in common.

Variable	C_1	C_2
(1-T)	$(-\frac{5}{2}+\frac{\pi^2}{3})C_F = 1.053$	-42 ± 22
$M_H/\sqrt{s}$	$(-\frac{5}{2}+\frac{\pi^2}{3})C_F = 1.053$	-48 ± 20
B_T	$(-\frac{17}{2}+\pi^2)C_F = 1.826$	-126 ± 16
B_W	$(-\frac{17}{2}+\pi^2)C_F = 1.826$	-182 ± 8
Σ_{EEC}	$(-\frac{11}{2}-\frac{\pi^2}{3})C_F = -11.72$	–
R_2	$(-\frac{5}{2}+\frac{\pi^2}{6}-6\ln 2)C_F = -6.69$	–

Variable	G_{12}	G_{11}	G_{23}	G_{22}	G_{21}
(1-T)	$-2C_F$	$3C_F$	$-\frac{11}{3}C_FC_A+\frac{2}{3}C_Fn_f$	$-\frac{4}{3}\pi^2C_F^2+(\frac{\pi^2}{3}-\frac{169}{36})C_FC_A+\frac{11}{18}C_Fn_f$	$+30 \pm 8$
	$=-\frac{8}{3}$	$=+4$	$=-10.22$	$=-24.94$	
$M_H/\sqrt{s}$	$-2C_F$	$3C_F$	$-\frac{11}{3}C_FC_A+\frac{2}{3}C_Fn_f$	$-\frac{2}{3}\pi^2C_F^2+(\frac{\pi^2}{3}-\frac{169}{36})C_FC_A+\frac{11}{18}C_Fn_f$	$+36 \pm 11$
	$=-\frac{8}{3}$	$=+4$	$=-10.22$	$=-13.24$	
B_T	$-4C_F$	$6C_F$	$-\frac{88}{9}C_FC_A+\frac{16}{9}C_Fn_f$	$-\frac{16}{3}\pi^2C_F^2+(\frac{2\pi^2}{3}-\frac{35}{9})C_FC_A+\frac{2}{9}C_Fn_f$	$+201 \pm 16$
	$=-\frac{16}{3}$	$=+8$	$=-27.26$	$=-81.33$	
B_W	$-4C_F$	$6C_F$	$-\frac{88}{9}C_FC_A+\frac{16}{9}C_Fn_f$	$-\frac{8}{3}\pi^2C_F^2+(\frac{2\pi^2}{3}-\frac{35}{9})C_FC_A+\frac{2}{9}C_Fn_f$	$+219 \pm 8$
	$=-\frac{16}{3}$	$=+8$	$=-27.26$	$=-34.55$	
Σ_{EEC}	$-C_F$	$3C_F$	$-\frac{11}{9}C_FC_A+\frac{2}{9}C_Fn_f$	$(\frac{\pi^2}{6}-\frac{35}{36})C_FC_A+\frac{1}{18}C_Fn_f$	-58 ± 7
	$=-\frac{4}{3}$	$=+4$	$=-3.41$	$=3.06$	
R_2	$-C_F$	$3C_F$	$-\frac{11}{9}C_FC_A+\frac{2}{9}C_Fn_f$	$\frac{11}{4}C_FC_A-\frac{1}{2}C_Fn_f$	–
	$=-\frac{4}{3}$	$=+4$	$=-3.41$	$=7.67$	

Table 3: QCD coefficients used in the matching of the NLLA and $\mathcal{O}(\alpha_s^2)$ QCD calculations. For QCD $C_F = \frac{4}{3}$, $C_A = 3$ and n_f is taken to be 5. The C_1 coefficients take into account the difference between the Born and the $\mathcal{O}(\alpha_s)$ hadronic cross-section. Coefficients derived from fits to the full $\mathcal{O}(\alpha_s^2)$ coefficient $\mathcal{B}(y)$ are shown with errors. In the cases where coefficients are unknown they were taken to be zero.

Variable	NLLA+$\mathcal{O}(\alpha_s^2)$ fits	$\mathcal{O}(\alpha_s^2)$ fits
(1-T)	0.06 – 0.30	0.08 – 0.30
$M_H/\sqrt{s}$	0.18 – 0.40	0.20 – 0.52
B_T	0.09 – 0.23	0.14 – 0.28
B_W	0.07 – 0.17	0.08 – 0.21
Σ_{EEC} : χ	43.2° – 162.0°	43.2° – 162.0°
R_2 : y_{cut}	0.005 – 0.20	0.01 – 0.20
$\mathcal{N}$: y_{cut}	0.005–0.05	0.02–0.10

Table 4: Ranges used for QCD fits to the data.

	(1-T)	M_H	B_T	B_W	Σ_{EEC}	R_2	$\mathcal{N}$
$\boldsymbol{x_\mu = 1}$							
$\Lambda_{\overline{MS}}$ (MeV)	267 ± 7	246 ± 6	259 ± 6	139 ± 4	459 ± 4	289 ± 7	285 ± 5
$\alpha_s(M_{Z^0})$	0.1211	0.1195	0.1197	0.1099	0.1322	0.1225	0.1226
χ^2/d.o.f.	2.3	9.4	5.1	18.8	6.5	6.8	2.4
$\boldsymbol{x_\mu}$ **fitted**							
$\Lambda_{\overline{MS}}$ (MeV)	990^{+790}_{-370}	162 ± 9	92 ± 7	80 ± 2	568 ± 8	900^{+600}_{-320}	316 ± 6
$\alpha_s(M_{Z^0})$	0.1521	0.1124	0.1040	0.1021	0.1372	0.1493	0.1246
x_μ	$10.0^{+15.2}_{-5.4}$	0.34±0.04	0.13±0.03	0.17±0.01	1.89±0.09	$23.6^{+48.1}_{-14.2}$	1.37±0.25
χ^2/d.o.f.	1.9	4.5	2.6	2.0	3.5	5.1	0.7

Table 5: Results of fitting the NLLA+$\mathcal{O}(\alpha_s^2)$ QCD calculations to the data, using the $\ln(R)$-matching scheme in all cases except Σ_{EEC}, where the modified R scheme is used.

	(1-T)	M_H	B_T	B_W	Σ_{EEC}	R_2	$\mathcal{N}$
$\boldsymbol{x_\mu = 1}$							
$\Lambda_{\overline{MS}}$ (MeV)	532 ± 16	386 ± 10	630 ± 19	354 ± 10	348 ± 3	277 ± 8	378 ± 12
$\alpha_s(M_{Z^0})$	0.1356	0.1284	0.1397	0.1266	0.1263	0.1217	0.1283
χ^2/d.o.f.	7.4	18.4	2.7	10.3	9.7	4.4	10.4
$\boldsymbol{x_\mu}$ **fitted**							
$\Lambda_{\overline{MS}}$ (MeV)	146 ± 7	219 ± 5	445^{+69}_{-57}	209 ± 7	181 ± 6	193 ± 11	203 ± 6
$\alpha_s(M_{Z^0})$	0.1107	0.1174	0.1315	0.1166	0.1141	0.1152	0.1164
x_μ	0.055±0.007	0.071±0.004	$0.59^{+0.14}_{-0.11}$	0.070±0.006	0.18±0.01	0.092±0.015	0.067±0.014
χ^2/d.o.f.	2.4	3.0	2.5	2.4	7.8	1.8	0.4

Table 6: Results of fitting the $\mathcal{O}(\alpha_s^2)$ QCD calculations to the data.

	(1-T)	M_H	B_T	B_W	Σ_{EEC}	R_2	$\mathcal{N}$
$\ln(R)$-matching : $\alpha_s(M_{Z^0})$	0.1211	0.1195	0.1197	0.1099	–	0.1225	0.1226
: χ^2/d.o.f.	2.3	9.4	5.1	18.8		6.8	2.4
R-matching : $\alpha_s(M_{Z^0})$	0.1243	0.1243	0.1279	0.1203	0.1283	0.1120	0.1280
: χ^2/d.o.f.	1.6	27.5	226.	250.	4.3	26.9	9.4
Modified R-matching : $\alpha_s(M_{Z^0})$	0.1209	0.1192	0.1229	0.1116	0.1322	–	–
: χ^2/d.o.f.	1.8	12.5	7.7	19.7	6.5		
Modified $\ln(R)$ matching : $\alpha_s(M_{Z^0})$	0.1207	0.1190	0.1189	0.1099	–	0.1226	–
: χ^2/d.o.f.	5.5	4.7	2.2	2.6		6.6	

Table 7: Values of $\alpha_s(M_{Z^0})$ and χ^2/d.o.f. derived by fitting the NLLA+$\mathcal{O}(\alpha_s^2)$ QCD calculations to the data, for $x_\mu = 1$, using different matching schemes. As explained in the text, the matching schemes have a slightly different meaning for $\mathcal{N}$.

	(1-T)	M_H	B_T	B_W	Σ_{EEC}	R_2	$\mathcal{N}$
$\alpha_s(M_{Z^0})$	**0.1211**	**0.1195**	**0.1197**	**0.1099**	**0.1322**	**0.1225**	**0.1226**
Statistical	$\pm$0.0005	$\pm$0.0005	$\pm$0.0005	$\pm$0.0004	$\pm$0.0002	$\pm$0.0005	$\pm$0.0003
Experimental Syst.	$\pm$0.0024	$\pm$0.0017	$\pm$0.0032	$\pm$0.0026	$\pm$0.0031	$\pm$0.0042	$\pm$0.0034
JETSET / a + 1 s.d.	$-$0.0006	$-$0.0022	$-$0.0013	$-$0.0004	$-$0.0014	+0.0002	+0.0002
JETSET / a $-$ 1 s.d.	+0.0006	+0.0009	+0.0009	0.0000	+0.0005	$-$0.0001	$-$0.0002
JETSET / σ_q + 1 s.d.	$-$0.0006	$-$0.0005	$-$0.0006	$-$0.0007	$-$0.0008	+0.0001	+0.0001
JETSET / σ_q $-$ 1 s.d.	+0.0020	+0.0010	+0.0018	+0.0003	+0.0009	+0.0002	+0.0001
JETSET / Peterson	+0.0010	+0.0010	$-$0.0006	$-$0.0003	+0.0005	+0.0014	+0.0014
JETSET / udsc only	+0.0022	+0.0003	+0.0042	+0.0020	+0.0017	+0.0026	+0.0025
JETSET / $Q_0 = 2$ GeV	$-$0.0012	+0.0001	$-$0.0008	+0.0001	$-$0.0009	+0.0016	+0.0019
HERWIG 5.5	$-$0.0040	+0.0031	$-$0.0090	$-$0.0014	$-$0.0041	+0.0018	+0.0052
ARIADNE 3.1	+0.0005	+0.0018	$-$0.0022	+0.0004	$-$0.0012	$-$0.0042	$-$0.0024
COJETS 6.23	$-$0.0357	$-$0.0235	$-$0.0399	$-$0.0275	$-$0.0404	$-$0.0247	$-$0.0202
Total Hadronization	$\pm$0.0053	$\pm$0.0044	$\pm$0.0105	$\pm$0.0026	$\pm$0.0050	$\pm$0.0057	$\pm$0.0067
$x_\mu = 0.5$	$-$0.0058	$-$0.0050	$-$0.0066	$-$0.0039	$-$0.0045	+0.0019	$-$0.0035
$x_\mu = 2$	+0.0072	+0.0066	+0.0080	+0.0049	+0.0054	+0.0023	+0.0048
Total error	$^{+0.0093}_{-0.0082}$	$^{+0.0082}_{-0.0069}$	$^{+0.0136}_{-0.0128}$	$^{+0.0061}_{-0.0054}$	$^{+0.0080}_{-0.0074}$	$^{+0.0075}_{-0.0073}$	$^{+0.0089}_{-0.0083}$

Table 8: Systematic errors on the value of $\alpha_s(M_{Z^0})$ derived from each of the seven observables. In all cases the NLLA+$\mathcal{O}(\alpha_s^2)$ QCD calculations were fitted to the data assuming $x_\mu = 1$. The $\ln(R)$-matching scheme was used except for Σ_{EEC}, where the modified R-scheme was taken. In the cases where a signed value is quoted, this indicates the direction in which $\alpha_s(M_{Z^0})$ changed with respect to the default analysis when a certain feature of the analysis was changed.

	(1-T)	M_H	B_T	B_W	Σ_{EEC}
$\ln(R)$-matching : $\alpha_s(M_{Z^0})$	0.1195	0.1208	0.1212	0.1133	–
: χ^2/d.o.f.	1.5	3.4	1.5	1.5	
: G_{32}	-370 ± 85	575 ± 70	1330 ± 180	2380 ± 170	
Modified R-matching : $\alpha_s(M_{Z^0})$	0.1200	0.1206	0.1249	0.1149	0.1300
: χ^2/d.o.f.	1.6	4.3	1.4	1.5	4.4
: G_{32}	-190 ± 80	670 ± 70	1650 ± 170	2420 ± 170	-210 ± 20
Modified $\ln(R)$ matching : $\alpha_s(M_{Z^0})$	0.1175	0.1198	0.1179	0.1111	–
: χ^2/d.o.f.	1.5	2.6	1.2	1.0	
: G_{32}	-725 ± 85	315 ± 65	-640 ± 190	590 ± 150	

Table 9: Values of $\alpha_s(M_{Z^0})$ and χ^2/d.o.f. derived by fitting the NLLA+$\mathcal{O}(\alpha_s^2)$ QCD calculations to the data, for $x_\mu = 1$, allowing the subleading coefficient G_{32} to be determined in the fit.

	$\alpha_s(M_{Z^0})$ NLLA+$\mathcal{O}(\alpha_s^2)$	$\alpha_s(M_{Z^0})$ $\mathcal{O}(\alpha_s^2)$ only
$(1-T)$	$0.121^{+0.009}_{-0.008}$	0.123±0.013
M_H	$0.119^{+0.008}_{-0.007}$	0.123±0.007
B_T	$0.120^{+0.014}_{-0.013}$	0.136±0.015
B_W	$0.110^{+0.006}_{-0.005}$	0.122±0.007
Σ_{EEC}	$0.132^{+0.008}_{-0.007}$	0.120±0.009
R_2	0.122±0.007	0.119±0.010
$\mathcal{N}$	$0.123^{+0.009}_{-0.008}$	0.122±0.012
Weighted Mean	0.120±0.006	0.122±0.007

Table 10: Summary of values of $\alpha_s(M_{Z^0})$ derived from each of the seven observables using the NLLA+$\mathcal{O}(\alpha_s^2)$ QCD calculations. Values based on simple $\mathcal{O}(\alpha_s^2)$ QCD are given for comparison.

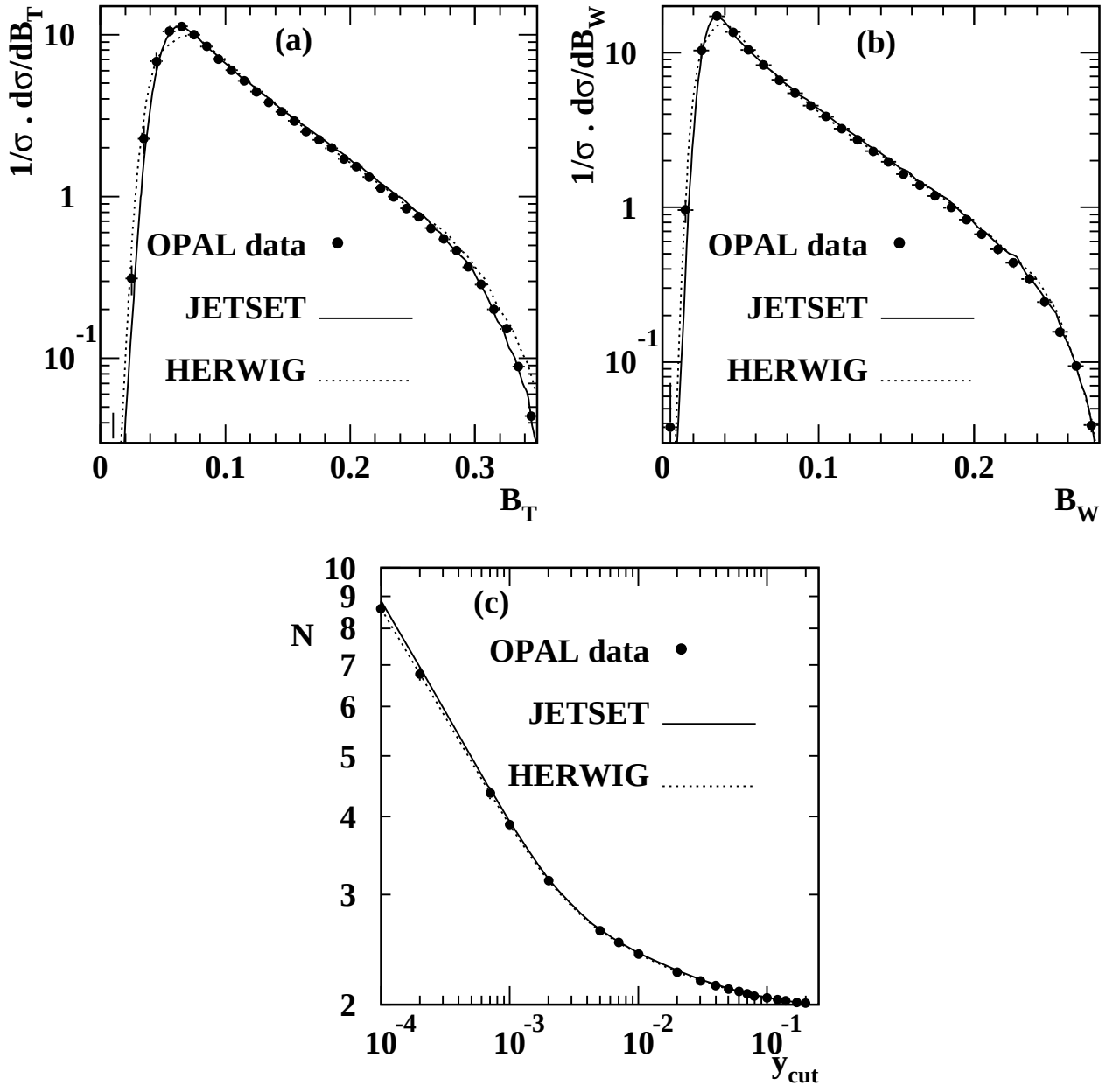

Figure 1: Data corrected to the hadron level for: (a) B_T, (b) B_W, (c) $\mathcal{N}$. The curves show the predictions of the QCD parton shower models JETSET (solid) and HERWIG (dotted) as described in the text.

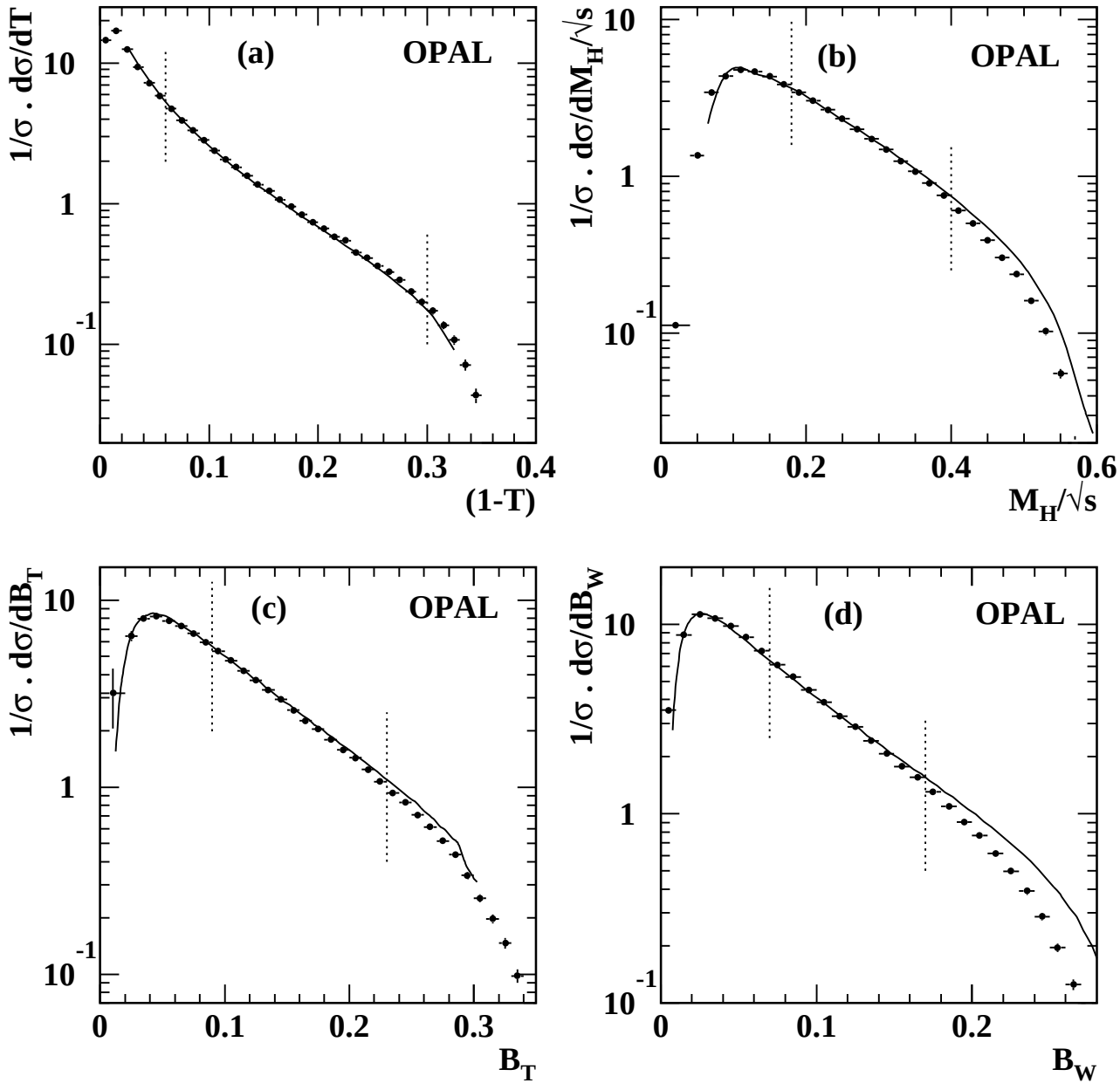

Figure 2: Normalized cross-sections $\frac{1}{\sigma}\frac{d\sigma}{dX}$, corrected to the parton level, where the observable X is: (a) $(1-T)$, (b) $M_H/\sqrt{s}$, (c) B_T, (d) B_W. The curves show the QCD fits using NLLA+$\mathcal{O}(\alpha_s^2)$ calculations combined with $\ln(R)$-matching, at scale x_μ=1. The dotted lines indicate the fit ranges used.

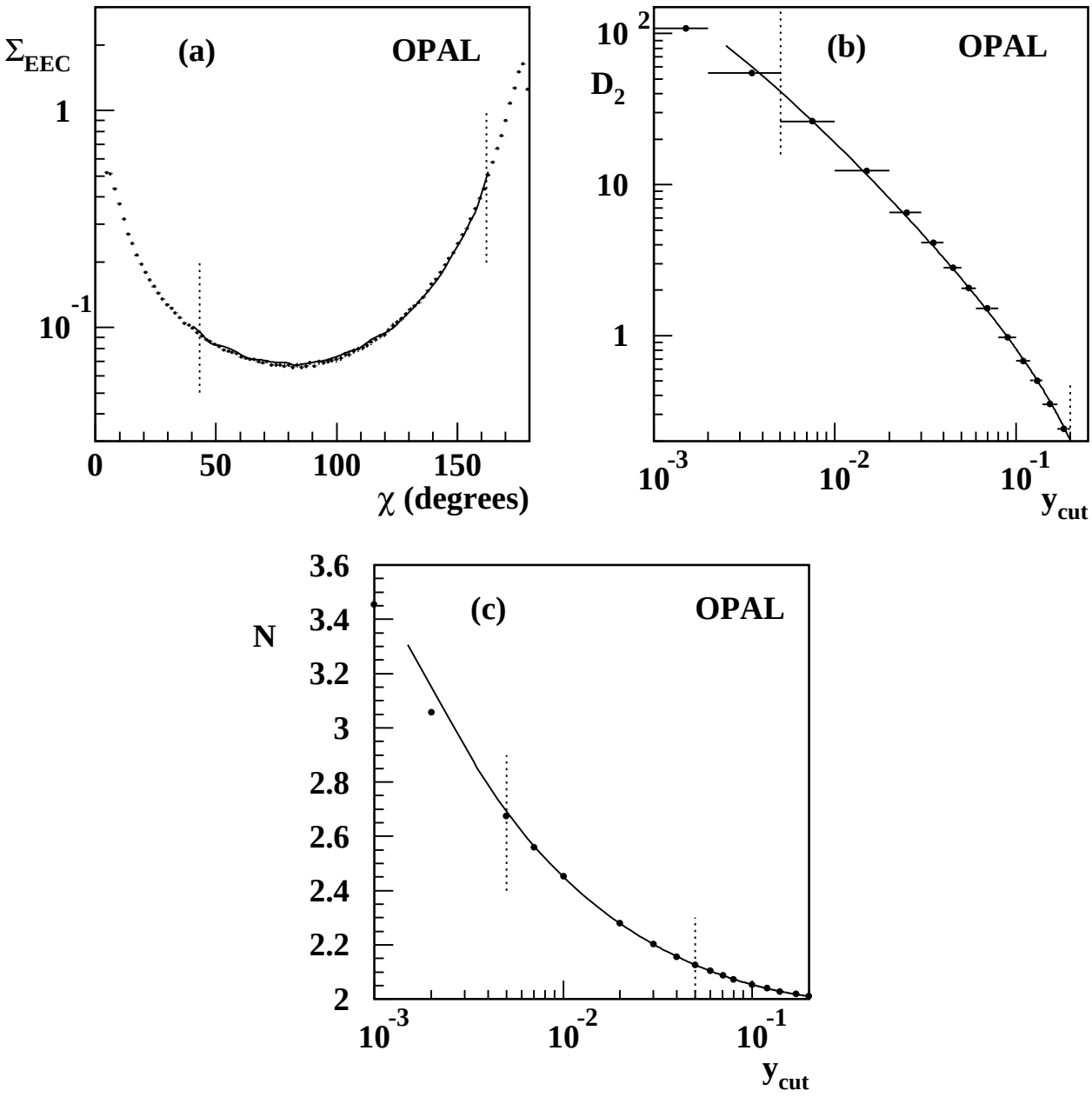

Figure 3: Data corrected to the parton level for: (a) Σ_{EEC}, (b) R_2, (c) $\mathcal{N}$. The curves show the QCD fits using NLLA+$\mathcal{O}(\alpha_s^2)$ calculations combined with $\ln(R)$-matching, or modified R-matching in the case of Σ_{EEC}, at scale x_μ=1. The dotted lines indicate the fit ranges used.

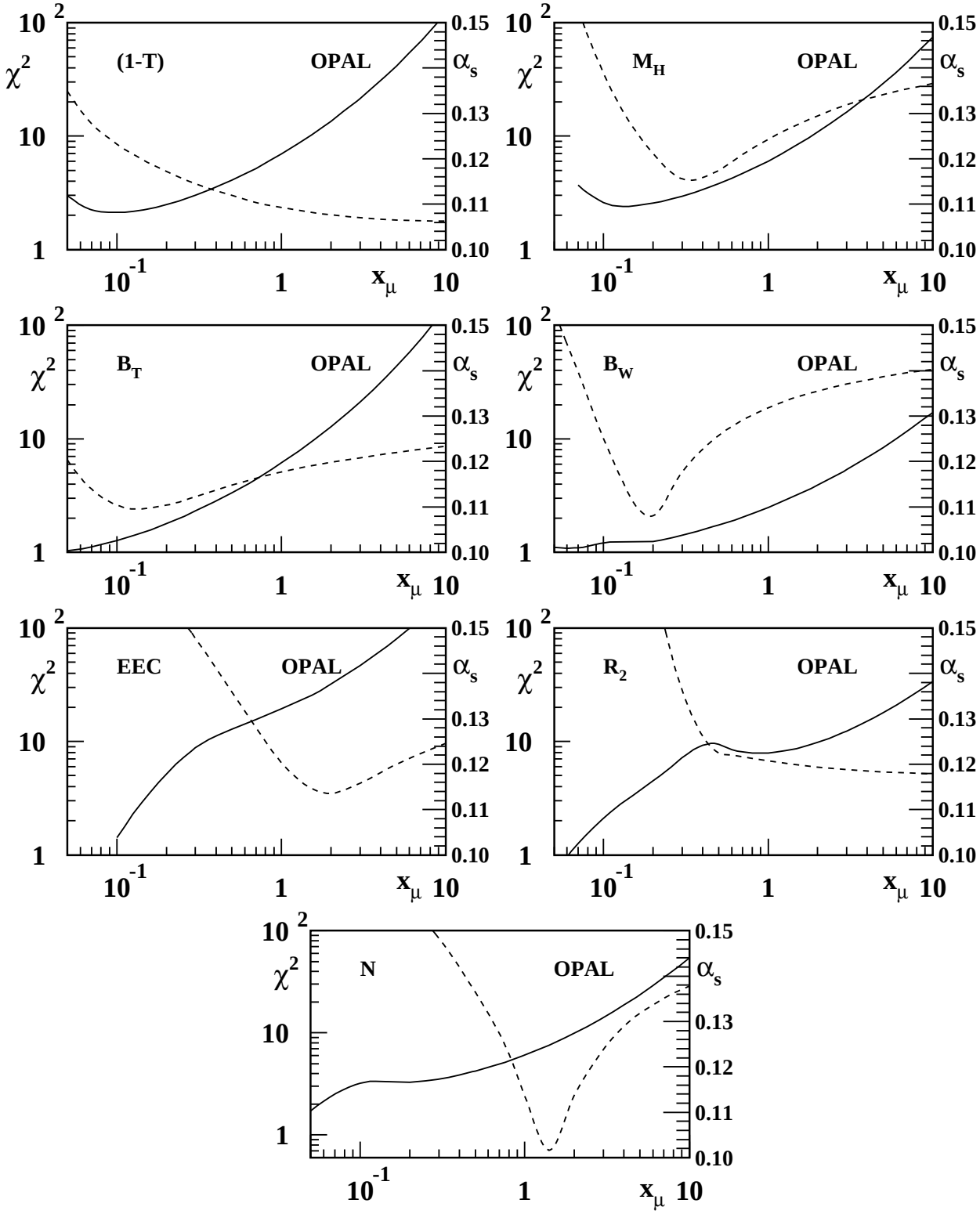

Figure 4: Dependence of $\alpha_s(M_{\mathrm{Z}^0})$ (solid curves) and χ^2/d.o.f. (dashed curves) on x_μ for NLLA+$\mathcal{O}(\alpha_s^2)$ fits to the OPAL data. In all cases $\ln(R)$-matching was used, with the exception of Σ_{EEC}, for which modified R-matching was chosen.

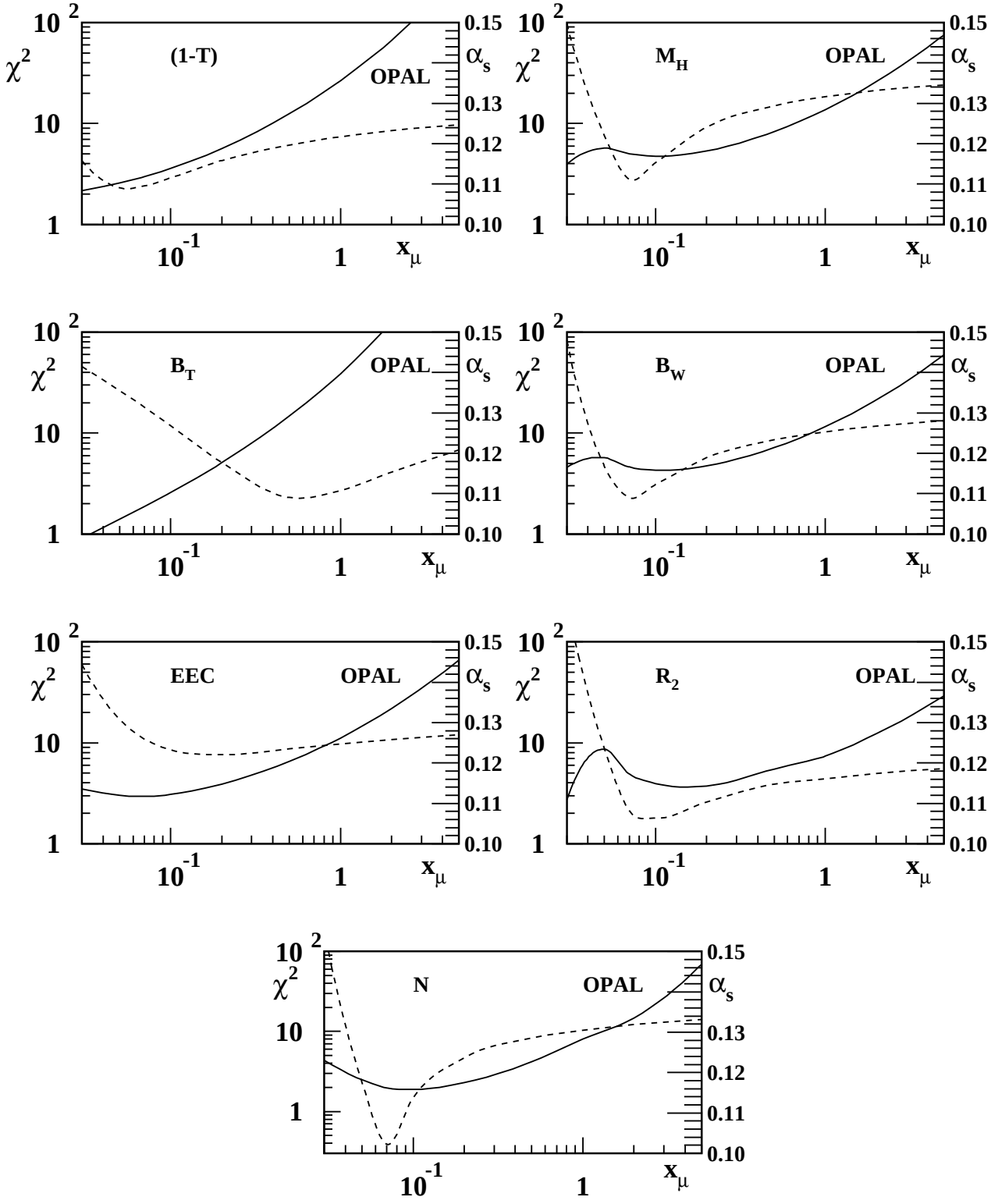

Figure 5: Dependence of $\alpha_s(M_{Z^0})$ (solid curves) and χ^2/d.o.f. (dashed curves) on x_μ for $\mathcal{O}(\alpha_s^2)$ fits to the OPAL data.

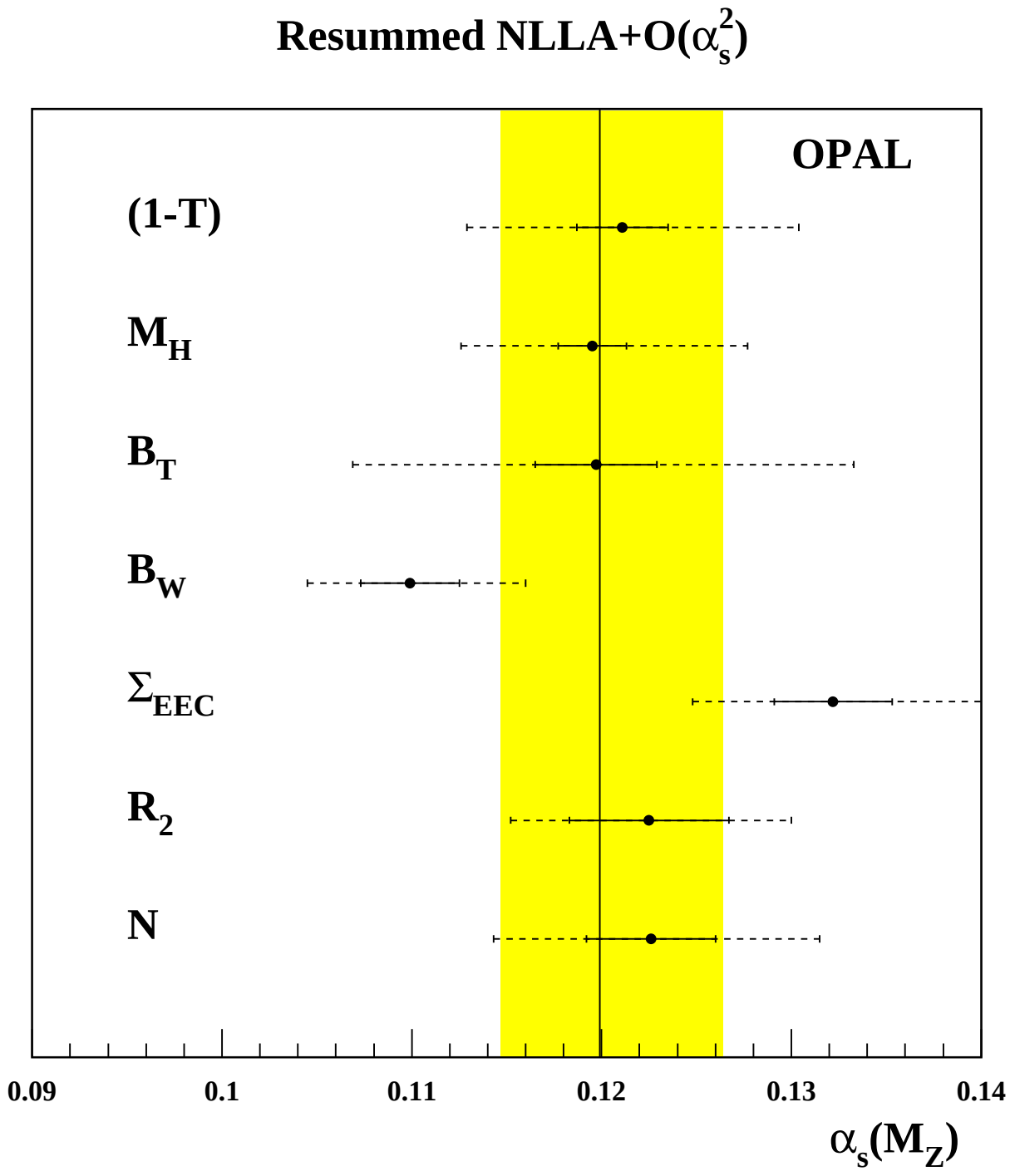

Figure 6: Values of $\alpha_s(M_{Z^0})$ derived from NLLA+$\mathcal{O}(\alpha_s^2)$ fits to the OPAL data. The solid error bars denote the experimental uncertainties, while the dashed error bars show the total errors, including hadronization and higher order effects. The vertical line and the shaded region represent the weighted mean value and its error.

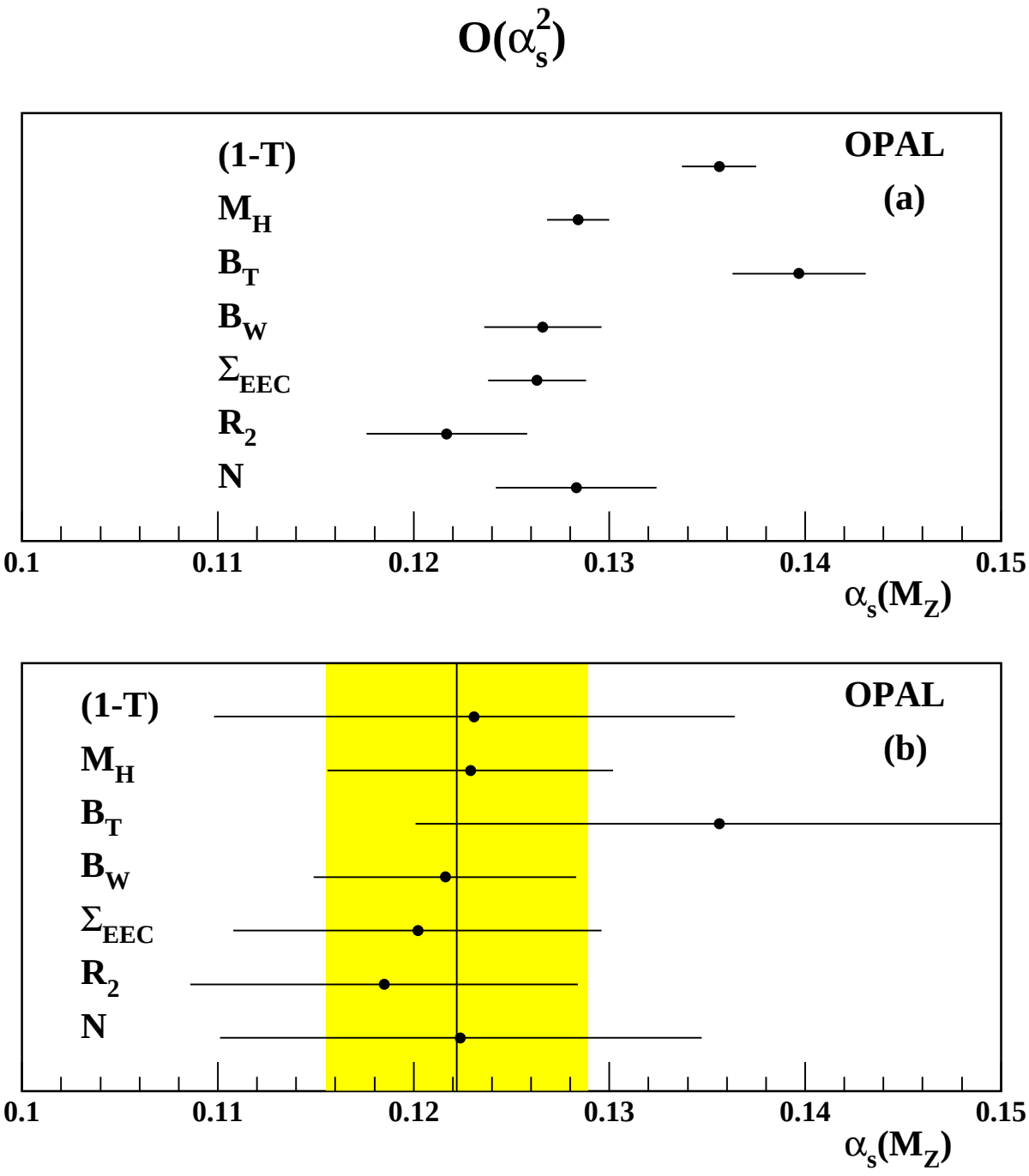

Figure 7: Values of $\alpha_s(M_{Z^0})$ derived from $\mathcal{O}(\alpha_s^2)$ fits to the OPAL data: (a) values at x_μ=1, where the error bars denote the experimental uncertainties only, (b) values based on the average of x_μ=1 and optimised x_μ, where the total errors, including hadronization and higher order effects, are shown. The vertical line and the shaded region represent the weighted mean value and its error.